CEAS Space Journal (2026) 18:121–144
https://doi.org/10.1007/s12567-025-00625-8

ORIGINAL PAPER

# Comparison of SpaceX's Starship with winged heavy-lift launcher options for Europe

**Moritz Herberhold[1] · Leonid Bussler[1] · Martin Sippel[1] · Jascha Wilken[1]**

Received: 4 March 2025 / Revised: 24 April 2025 / Accepted: 5 May 2025 / Published online: 28 May 2025
© The Author(s) 2025

**Abstract**
The remarkable progress SpaceX made in the first four integrated flight tests of their Starship and Super Heavy launcher configuration indicates that a fully reusable space transport system might become a reality within a few years. Such a system could revolutionize the global launch market, especially if it is able to achieve its forecasted payload capacity of more than 100 t into LEO. Therefore, it is necessary to gain a deep understanding of the capabilities of this system and compare it to potential future European options for heavy and super-heavy space transport systems. This paper uses the publicly available data from Starship's first four integrated flight tests for a thorough technical analysis of its current capabilities. The flight tests allow a calibration and update of our earlier-presented Starship models with real flight data. These updated models will be used to gain an understanding of its high-level system properties and to extrapolate the actual LEO capabilities of the early operational Starship versions. The second part of the paper will investigate a potential European option for launching similar payloads of 50 t and more into LEO, based on building blocks currently proposed or under investigation. This configuration employs a reusable winged first stage based on the SpaceLiner concept's booster stage. The stage uses cryogenic liquid hydrogen and cryogenic liquid oxygen and is recovered with in-air capturing (IAC). For the second stage, an expendable cryogenic stage is optimized to maximize the payload capacity. Finally, the paper compares the technical characteristics of the presented winged launch vehicle to the Starship's capabilities to highlight the key advantages of the two differing approaches and identify promising future development roadmaps for European launchers.

**Keywords** Heavy-Lift Launchers · Reusable · VTHL · VTVL · Starship · SpaceLiner

**Abbreviations**

| | |
|---|---|
| AoA | Angle of attack |
| MCCP | Main combustion chamber pressure |
| DLR | German Aerospace Center |
| ET | Space shuttle external tank |
| FFSC | Full-flow staged combustion |
| GLOW | Gross lift-off weight |
| HRSI | High-temperature reusable surface insulation |
| IAC | In-air capturing |
| IFT | Integrated flight test |
| $I_{SP\,sp}$ | Specific impulse |
| LEO | Low earth orbit |
| Max Q | Point of maximum dynamic pressure |
| MECO | Main engine cut-off |
| MR | Mixture ratio |
| RTLS | Return to launch site |
| SART | Space Launcher System Analysis Department |
| SECO | Second-stage engine cut-off |
| SI | Structural index |
| SLB | SpaceLiner booster |
| SLME | SpaceLiner main engine |
| TWR | Thrust-to-weight ratio |
| VTVL | Vertical take-off vertical landing |

✉ Moritz Herberhold
moritz.herberhold@dlr.de

[1] Deutsches Zentrum Für Luft- Und Raumfahrt, Institut Für Raumfahrtsysteme, Robert-Hooke-Straße 7, 28359 Bremen, Germany

## 1 Introduction

The rapid advancements in space transportation technology, particularly through SpaceX's development of the Starship and Super Heavy launch system, have the potential to revolutionize the global launch market. With its projected payload capacity exceeding 100 metric tons to low earth orbit (LEO) while being fully reusable [1], Starship represents a significant leap forward in space transport. Such a development

necessitates a rigorous technical evaluation to understand its capabilities and potential impact on future space operations. Furthermore, as Europe continues to develop its own space launch capabilities, it is crucial to evaluate emerging technologies like Starship against potential European alternatives in the heavy and super-heavy launch vehicle categories.

Through a multidisciplinary technical assessment and system-level comparison, this paper aims to support future launcher development by examining Starship alongside a European reusable alternative. It also demonstrates the use of consistent modeling frameworks for the comparison of different launcher architectures and introduces a methodology to validate Starship models with real flight data. In addition, by contrasting two distinct reusability approaches—full versus partial—it contributes to a deeper understanding of how reusability influences the design and performance of super-heavy launch vehicles.

Specifically, it offers a thorough technical analysis of SpaceX's Starship in Chapter 2. It updates and extends the published mass, engine and aerodynamic models [2] using the newest publicly available information. It further validates the models by matching real flight data from the first integrated flight tests (IFTs) with trajectory simulations. This approach ensures that the models reflect the Starship's real-world performance and allows a realistic characterization of its operational capabilities and payload performance.

In parallel, Chapter 3 explores a conceptual European alternative for heavy-lift and super-heavy-lift missions, based on building blocks currently under investigation as part of the SpaceLiner concept [3, 4]. The proposed configuration integrates the SpaceLiner's reusable, winged first stage [5], with an expendable cryogenic upper stage to deliver payloads of over 50 t to LEO.

The comparative study in Chapter 4 of Starship and the proposed European alternative highlights the strengths and trade-offs between the fully reusable and partially reusable architectures. By evaluating their technological and operational differences, this study aims to inform ongoing discussions about future strategic directions in European space transportation.

## 2 SpaceX Starship

With the recent seven integrated flight tests (IFTs) of SpaceX's Starship and Super Heavy, the company shows that they come ever closer to realizing the world's first fully reusable space transport system. The system, shown in Fig. 1, has a maximum lift-off mass beyond 5000 t. A total of 33 Raptor 2 full-flow staged combustion (FFSC) cycle engines provide more than 70.000 kN of thrust for the first stage, while six additional Raptor 2 engines propel the second stage onto its final orbit. With a projected payload capacity of 100 tons or more to LEO while being fully reusable, this system has the potential to transform the global launch market. [1]

**Fig. 1** Starship and Super Heavy before IFT 1. CC BY-NC 2.0. Source: SpaceX [6]

This chapter will analyze the high-level system properties of the Starship and Super Heavy based on publicly available data from the first four IFTs and use the derived models to extrapolate the future capabilities of the Starship.

### 2.1 Model description

Given the immense potential of the Starship, the German Aerospace Center's Space Launcher Systems Analysis Department (DLR-SART) has published several analyses of the configuration and its prior iterations. In 2018, an interim version of the system, the BFR, was thoroughly studied [7]. A detailed remodeling and analysis of the current Starship and Super Heavy configuration followed in 2022 [8], alongside an analysis of its point-to-point

capabilities [2]. However, since 2022, many changes have been introduced to the configuration and additional information became publicly available, allowing an update of the models. Furthermore, the telemetry data from the first four IFTs has provided the opportunity to verify the models with real flight data.

The following chapter will give a short overview of the current models and will describe the changes introduced since 2022 in more detail. A comprehensive description of the original model is provided in the 2022 analysis [8]. The Starship remains in its prototyping phase and hundreds of changes are applied between each test flight [9]. The Starship V1 and Super Heavy V1 models described in this paper aim to represent the IFT4 configuration of the Starship and Super Heavy, excluding changes made after IFT4. The enlarged future configuration Starship V2 and Super Heavy V2 [10] will be discussed in the later Chapter 2.4.2.

The remodeling of the Starship system employs various DLR-SART-internal numerical tools. These tools are specialized in the preliminary design of launch vehicles and provide rapid and accurate assessments of vehicle properties across several technical disciplines. The key equations used for the modeling can be found in the sources provided with the tools. The following SART numerical tools have been utilized in this work:

- **TOSCA** (Trajectory Optimization and Simulation of Conventional and Advanced spacecraft)—three-dimensional trajectory simulation and optimization [11].
- **STSM** (Space Transportation System Mass)—first level vehicle mass model generation.
- **PMP** (Propellant Management Program)—geometry generation and mass analysis for tanks, feed, fill-drain and pressurization lines [12].
- **TOP3** (Thermal Optimization Program 3)—tool for dimensioning the thermal protection system of space vehicles based on transient local 1D heat conduction [13].
- **HOTSOSE** (Hot Second Order Shock Expansion)—estimation of aerodynamic coefficients for hypersonic velocities (Ma > 5) using local surface inclination methods [14, 15].
- **GGH** (Grid Generation for HOTSOSE)—mesh generation for HOTSOSE.
- **CAC** (Computation of Aerodynamic Coefficients)—estimation of aerodynamic coefficients for subsonic, transonic and supersonic velocities (Ma < 5) using DATCOM methods [16].

Furthermore, the external tool RPA is used:

- **RPA** (Rocket Propulsion Analysis)—tool for performance prediction of rocket engines based on the Gibbs free energy minimization approach [17].

#### 2.1.1 Engine model

The SpaceX Raptor operates in full-flow staged-combustion (FFSC) cycle which is using the complete propellants to drive the turbopumps. Parsley et al. [18] explains the major thermodynamic advantage of FFSC as "*allowing a significant increase in the powerhead energy release within the same turbine temperature limits. […] The overall effect is approximately a 10% to 15% improvement in chamber pressure of the full-flow cycle over the conventional [Fuel Rich preburner] cycle combined with lower turbine temperatures.*". Raptor is the first FFSC rocket engine ever flown.

Since 2022, the Raptor 2 version is in production. In this version, the nominal chamber pressure has been raised to 300 bar, while its nozzle expansion ratio has been reduced. [19] The potential key objective for this design choice is to increase thrust of the engine without increasing the nozzle size. The constant nozzle size is required to fit the 33 engines in the available Super Heavy stage diameter of 9 m. Consequently, the nozzle exit diameter remained fixed at 1.3 m and the throat section must have been opened.

Precise engine performance data of the Raptor 2 has not been published. Therefore, the DLR performed an independent analysis of the Raptor 2 using the liquid rocket engine performance analysis tool RPA [17]. A SpaceX announcement of 230 tons (2260 kN) of sea-level thrust [20], a chamber pressure of 300 bar with an assumed mixture ratio of 3.6, and a nozzle exit diameter 1.3 m serve as guidelines for the calculation.

The nozzle expansion ratio has been slightly reduced to 32 instead of the previous 34.34 (probably as of Raptor 1). Recent data on Raptor 2, as published on Wikipedia [21], closely align with the calculations presented in Table 1. It should be noted that engine data collections on Wikipedia are to be treated with care and might contain inconsistencies or contradictions. Nevertheless, the Raptor 2 data based on DLR-calculations, while, at the same time, in overall

**Table 1** SpaceX raptor 2 engine (sea-level variant) calculated technical data

| | | |
|---|---|---|
| Mixture ratio [−] | 3.6 | |
| Assumed nozzle area ratio [−] | 32 | |
| Chamber pressure [bar] | 300 | 250 |
| Mass flow engine [kg/s] | 663.4 | 553.9 |
| Thrust at sea-level engine [kN] | 2123 | 1747 |
| Thrust in vacuum engine [kN] | 2260 | 1884 |
| $I_{SP}$ at sea level [s] | 326.4 | 321.6 |
| $I_{SP}$ in vacuum [s] | 347.4 | 346.8 |

agreement with references [20, 21], are a good working baseline for launch vehicle analyses. Shortly after lift-off, the Super Heavy and Starship configuration significantly throttles back to reduce loads in the maximum dynamic pressure regime (see Chapter 2.3.1). This change in mass flow might be achieved by adapting mixture ratio (MR), chamber pressure, or both. Conditions for the engines with the same thrust chamber geometry working at 250 bar are listed in the right column of Table 1 showing a reduction in sea-level thrust of almost 18% compared to the nominal value of 300 bar. The sensitivity of MR-variation on the Raptor 2 performance is depicted in Fig. 2.

The upper stage Raptor 2, featuring an enlarged nozzle, is referred to as RVAC by SpaceX. This engine has an exit diameter close to 2.3 m [21] considering pictures showing both Raptor variants integrated into the Starship base area. Thus, the nozzle geometry has been used again as a baseline assumption in combination with the reasonable hypothesis that other key parts of the engine (e.g., turbopumps, injector, throat) are similar to the sea-level variant. An expansion ratio of around 100 is consistent with the stated exit diameter. Table 2 lists key performance data of RVAC calculated under these constraints. According to SpaceX's website, the thrust should reach 258 tf (2530 kN) [1], approximately 6.3%

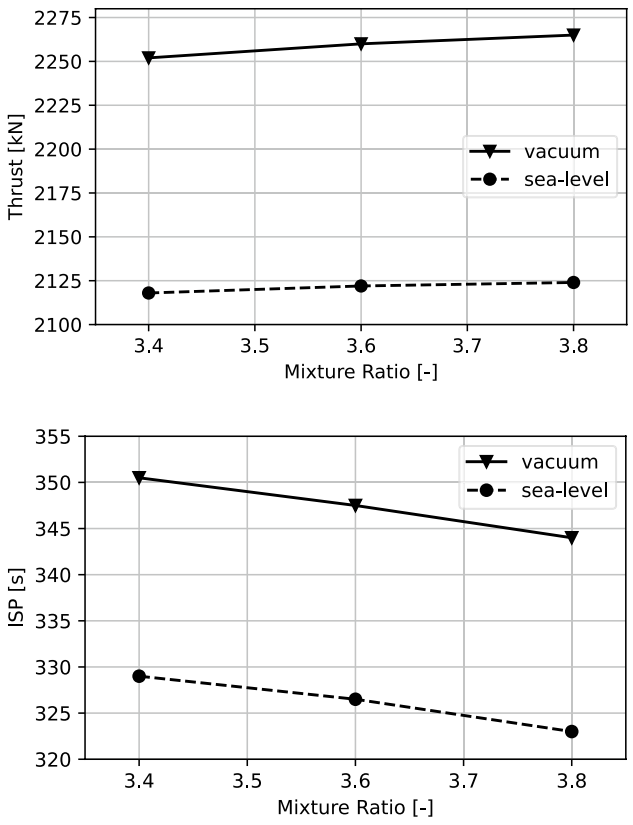


**Fig. 2** Raptor 2 engine (sea-level variant) performance depending on mixture ratio (chamber pressure 300 bar)

**Table 2** SpaceX raptor 2 RVAC engine (vacuum variant) calculated technical data

| | | |
|---|---|---|
| Mixture ratio [−] | 3.4 | 3.6 |
| Assumed nozzle area ratio [−] | 100 | |
| Chamber pressure [bar] | 300 | |
| Mass flow engine [kg/s] | 655.7 | 663.4 |
| Thrust in vacuum engine [kN] | 2369.6 | 2380.5 |
| $I_{SP}$ in vacuum [s] | 368.5 | 365.9 |

higher than computed. An explanation for this deviation is not readily available but turns out to be not critical for the accurate trajectory simulations in Sect. 2.2. The Starship employs three RVAC and three sea-level engines. Therefore, the parameters used for the simulation of the second stage are averaged, assuming identical mass flow rates for all six engines.

Recently, SpaceX announced the production start of its latest variant Raptor 3 [22] with the capability of operating at a very high chamber pressure of 350 bar. This engine supposedly incorporates innovative features, like regenerative cooling of all components while significantly simplifying the engine and increasing its thrust-to-weight ratio (TWR). Although, the functionality of the features is not yet exactly understood, nevertheless, an estimation of the engine's overall performance is possible assuming the same thrust chamber geometries as for Raptor 2 and a nominal chamber pressure of 350 bar.

Calculated thrust levels of Raptor 3 increase by 16.6% for the sea-level variant and by 15.6% for the upper stage engine. Any further increase is not compatible with the geometry constraints and announced chamber pressure. Therefore, the posted thrust [22] of 280 tf (2746.8 kN) is 4.98% above the calculated thrust at MR = 3.8. Further approaching stoichiometric conditions no longer increases thrust. Specific impulse ($I_{SP}$) at sea-level slightly increases relative to Raptor 2 while remaining almost constant in vacuum. The announced 350 s [22] are in line with calculations under realistic assumptions [23], including losses and typical mixture ratios.

Currently, not much is known about the motor's internal component characteristics. The cycle analyses reveal turbopump discharge pressures reaching or exceeding 1000 bar under the postulation of state-of-the-art efficiencies and valve or injector pressure losses. Though actual conditions inside Raptor are unknown, the challenge of successfully reaching such functional design under its severe thermal and mechanical loads becomes evident. The reduced engine weight of Raptor 3 as announced [22] compared to its predecessor is even more impressive if sustainable in day-to-day reusable operations.

Despite some deviations of the calculated thrust levels compared to published information on Raptor, the DLR

performance estimation is in overall good agreement. The preliminary engine mass estimations based on empirical relations for major subcomponents deliver significantly higher engine masses or lower TWR. The compact arrangement on Raptor and the inline LOX-powerhead are probably key elements for the achieved improvement. Both, DLR-estimated propulsion masses as well as SpaceX, published mass data are used in the vehicle performance assessments in Sect. 2.4.

### 2.1.2 Mass model

Central to Starship's and Super Heavy's mass models are tank and propellant feed system models created with the DLR-internal PMP tool. Visualizations of the models are provided in Figs. 3 and 4. The models are employed to calculate the mass of the propellant feed system and to estimate the necessary tank volume.

The Starship tank configuration consists of four stainless steel tanks. A mixture ratio of 3.4 : 1 is assumed, as this ratio provides a large vacuum ISP (see Table 2). The two main propellant tanks, a 790 $m^3$ oxygen tank and a 590 $m^3$ methane tank, are located in the vehicle's aft section, with the oxygen tank positioned below the methane tank. The oxygen header tank with a total volume of 19 $m^3$ is placed in the Starship's nose, while the smaller methane header tank with a volume of 17 $m^3$ sits at the internal bulkhead between the main tanks. Collectively, the modeled tanks fit 1200 t of subcooled cryogenic fuel, 30 t of which are located in the header tanks. The propellant feed system model contains the fuel lines to each of the six engines, as well as pressurization lines, which funnel heated gaseous fuel and oxygen from the engines back into the respective tanks.

Publicly available reconstructions and photographs [24] provide the basis for a detailed revision of the previously employed propellant feed system and tank model of the Super Heavy [8]. The Super Heavy tank model now consists of two primary tanks and a smaller LOX header tank, which is positioned within the main LOX tank. Here a higher mixture ratio of 3.6 : 1 is assumed to maximize the total thrust. The LCH4 tank is mounted atop the main LOX tank. LCH4 is initially directed through a central downcomer. This downcomer terminates in an LCH4 reservoir located at the base of the main LOX tank. The LOX header tank is positioned above the LCH4 reservoir. From this reservoir, individual fuel lines distribute LCH4 to each of the 33 engines. The main LOX lines directly connect all engines to the base of the LOX tank. In addition, the 13 inner engines are connected to the LOX header tank via secondary LOX lines, which are routed around and through the LCH4 reservoir. The model also includes pressurization lines from the engines back to the top of the tanks and fill and drain lines to the bottom of the LCH4 reservoir and primary LOX tank. A close view of the aft section of the Super Heavy and the propellant feed system model are shown in Fig. 5. The primary methane tank has a volume of 1740 $m^3$ and the primary oxygen tank has a volume of 2620 $m^3$.

For the remainder of the mass model, the DLR-internal tool STSM is used. This tool is capable of estimating the mass of common structures like tanks, electronics, or aerodynamic control surfaces, based on stochastic engineering methods. It also allows for the inclusion of fixed masses for components with publicly available mass information, like the Super Heavy's grid fins [9] and flame diverter [26]. The resulting mass model is shown in Table 3.

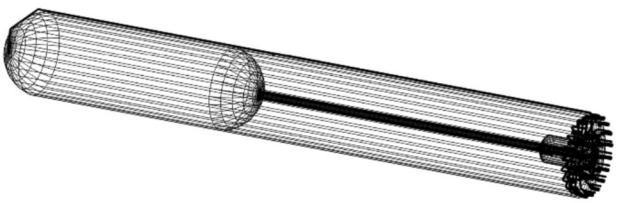

**Fig. 4** PMP propellant feed system and tank model of the Super Heavy V1

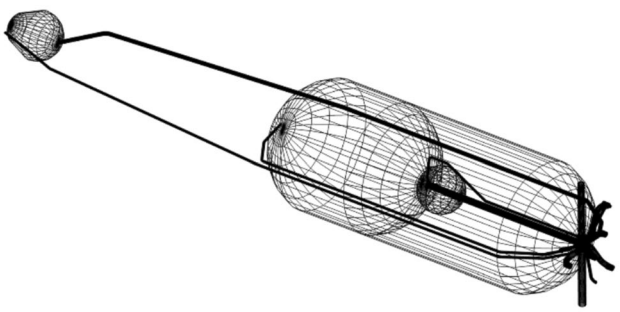

**Fig. 3** PMP propellant feed system and tank model of the Starship V1

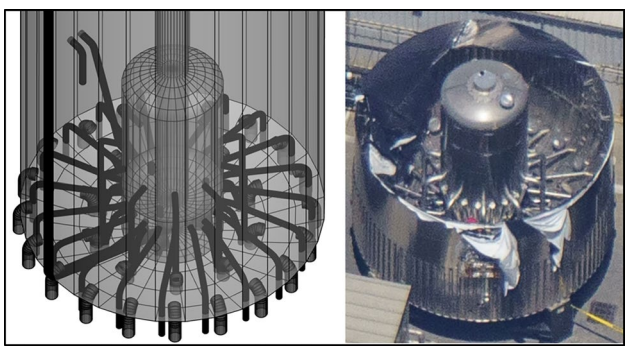

**Fig. 5** Comparison of the propellant feed system model with a close view of the aft section of the Super Heavy V1 [24] CC BY-NC 2.0. Source: RGV Aerial Photography [25]

**Table 3** Technical parameters of the V1 Starship and Super Heavy models

| | Starship V1 and Super Heavy V1 |
|---|---|
| 1st stage | |
| Propellant mass | 3300 t |
| Dry mass | 311 t |
| Structural index with propulsion | 9.4% |
| Structural index without propulsion | 6.2% |
| Total mass | 3611 t |
| Engine $I_{SP}$, sea level | 326 s |
| Engine $I_{SP}$, vacuum | 347 s |
| Tank volume | 4000 $m^3$ |
| Length | 71 m |
| Fuselage diameter | 9 m |
| 2nd stage | |
| Propellant mass | 1200 t |
| Dry mass | 118 t |
| Structural index with propulsion | 9.9% |
| Structural index without propulsion | 8.1% |
| Total mass | 1318 t |
| Engine $I_{SP}$, vacuum | 359 s |
| Tank volume | 1433 $m^3$ |
| Length | 50 m |
| Fuselage diameter | 9 m |
| Lift-off mass (without payload) | 4929 t |

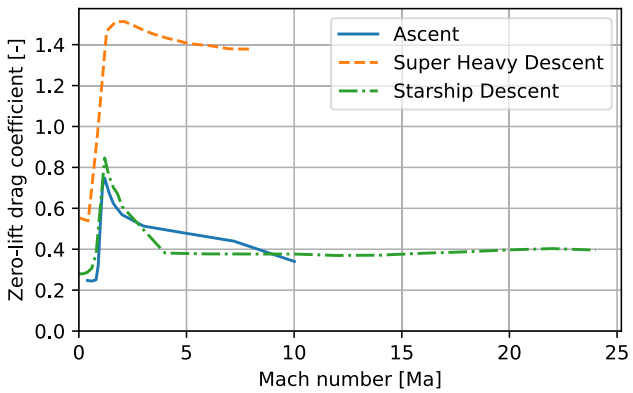


**Fig. 6** Zero-lift drag coefficient over Mach number for all three aerodynamic configurations

### 2.1.3 Aerodynamic model

In total, three aerodynamic models are utilized in the simulation of the Starship and Super Heavy. The zero-lift drag coefficients for all three models are shown in Fig. 6. All aerodynamic coefficients refer to the 63.82 $m^2$, circular cross-section of the configuration.

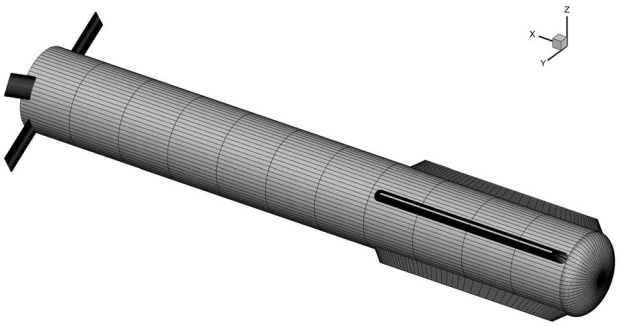

**Fig. 7** HOTSOSE aerodynamic grid of the Super Heavy V1 with simplified engine region

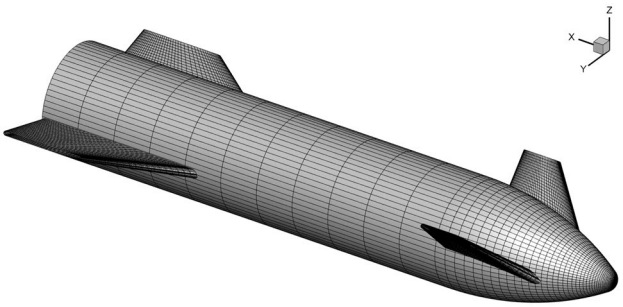

**Fig. 8** HOTSOSE aerodynamic grid of the Starship V1 with rear flaps at 10° and front flaps at 45°

For the ascent phase, a CAC model of the stacked configuration is employed. This model is also applied post-stage separation, as the aerodynamic forces during the second stage's ascent are minimal and no additional aerodynamic model is necessary.

For the descent of the Super Heavy, a combined aerodynamic model is used. For Ma ≥ 4, the DLR-internal tool HOTSOSE, based on surface inclination methods, is utilized. The used aerodynamic grid generated with GGH is depicted in Fig. 7. For $Ma < 4$, hand book methods based on DATCOM [27] are employed. The used methods are not able to represent the complex aerodynamics that form at the engine region. Therefore, the engine region is modeled by a simplified dome shape. The grid fins are also simplified to plates perpendicular to the flow, to represent their drag. The four chimes at the bottom of the booster are modeled by small fins. These primarily house pressure vessel, but might also be used to increase the booster's lift during reentry and, therefore, are present in this model. For a closer investigation, a simulation with computational fluid dynamics methods would be necessary.

The final model addresses Starship's aerodynamics during reentry. Again, HOTSOSE is used for Ma ≥ 4. Figure 8 illustrates the employed aerodynamic grid, generated with

GGH. During reentry, the vehicle is pitch-trimmed for maximum drag, with the center of gravity assumed to be positioned 25 m behind its nose. The trim is achieved by symmetrically adapting the canard and flap angle. The resulting trimmed lift and drag coefficients are shown in Fig. 9. Below Ma = 4, an untrimmed DATCOM aerodynamic dataset is used.

#### 2.1.4 Thermal protection system

The Starship's thermal protection system used during IFT4 [28] consists of roughly 33 mm thick hexagonal tiles, placed upon an insulation mat of roughly equal thickness. Each tile has a short diagonal diameter close to 24 cm and is attached to the steel hull via three welded-on steel pins. The thermal protection system completely covers the underside of the Starship's hull and fins. It partially covers the upper side around the nose and above the control surfaces. On the sides, 7–8 rows of tiles are placed above the middle line. The material composition of the tiles and the mat are not publicly known. Reports from the Florida Department of Environmental Protection [29] indicate that the tiles are sintered silica tiles with a reaction-cured glass glaze. Their production process is similar to the production process used

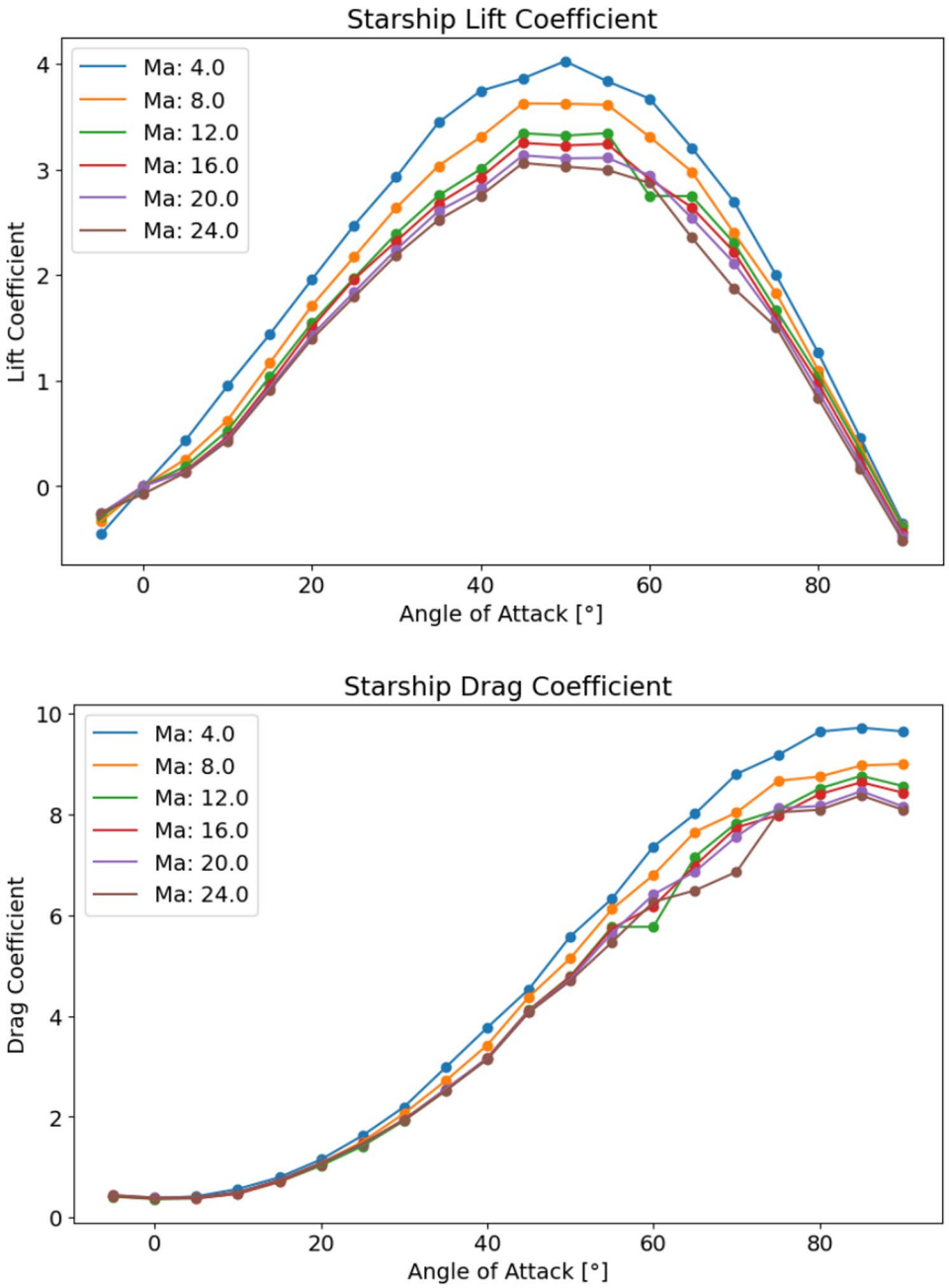


**Fig. 9** Lift and drag coefficients over angle of attack for the pitch-trimmed Starship V1 generated by HOTSOSE

for the high-temperature reusable surface insulation (HRSI) tiles [30] of the Space Shuttle orbiter, and thus, equivalent properties are assumed for the model, most importantly the surface temperature is limited to 1870 K. For the insulation mat, a lightweight ALTRA alumina mat [31] is assumed. To refine this assumption and evaluate its impact on the vehicle mass and center of gravity, the thermal protection system was sized in a dedicated analysis with the DLR-SART tool top3. The local material combinations are selected based on the maximum surface temperature while the thickness of insulating layers is calculated based on integration of the local 1D heat conduction into the vehicle. The heatshield is optimized to limit the maximum temperature of the structure beneath the heat shield to 700 K. For areas with surface temperatures below 700 K, no heatshield is used.

The combined mass of the tiles and mat is approximated to 8.7 kg/m$^3$. The steel pins are not represented in the thermodynamic model, but their mass is represented by an additional 1.5kg/m$^2$. Combined with a 15% margin, the total mass of the thermal protection system is estimated to be 10400 kg.

As stated in Chapter 2.1, the described model represents the Starship flown in IFT4. It is important to note that during IFT4's reentry, the Starship suffered extensive thermal damage [32], leading to a complete overhaul of the thermal protection system. The system that will be used for IFT5 and subsequent flights includes an ablative layer below the heat shield tiles [33], which adds additional mass.

## 2.2 Integrated flight tests

The following chapter describes the Starship's and Super Heavy's ascent, return, and reentry trajectories for IFT-2, IFT-3, and IFT-4. The used telemetry is extracted from the publicly available broadcasts [32, 34, 35] by a text recognition algorithm based on Chris Billington's [36] open source code. The telemetry is extracted at a rate of one datapoint per second.

### 2.2.1 Ascent

The speed and altitude telemetry for the ascent trajectories is presented in Fig. 10, which also includes a comparison with Tosca simulations. The ascent profiles of the three test flights exhibit significant similarities, allowing for a unified description. The key differences are pointed out within the description.

The Starship launches from SpaceX's Boca Chica facility in Texas, located at 25.996°N, 97.155°E, with an eastward trajectory slightly deflected southward to maintain a flight path over water through the Caribbean. Engine ignition occurs approximately three seconds before liftoff, followed by a vertical ascent lasting 15–20 s, achieving an initial TWR of 1.4. Subsequently, the rocket begins

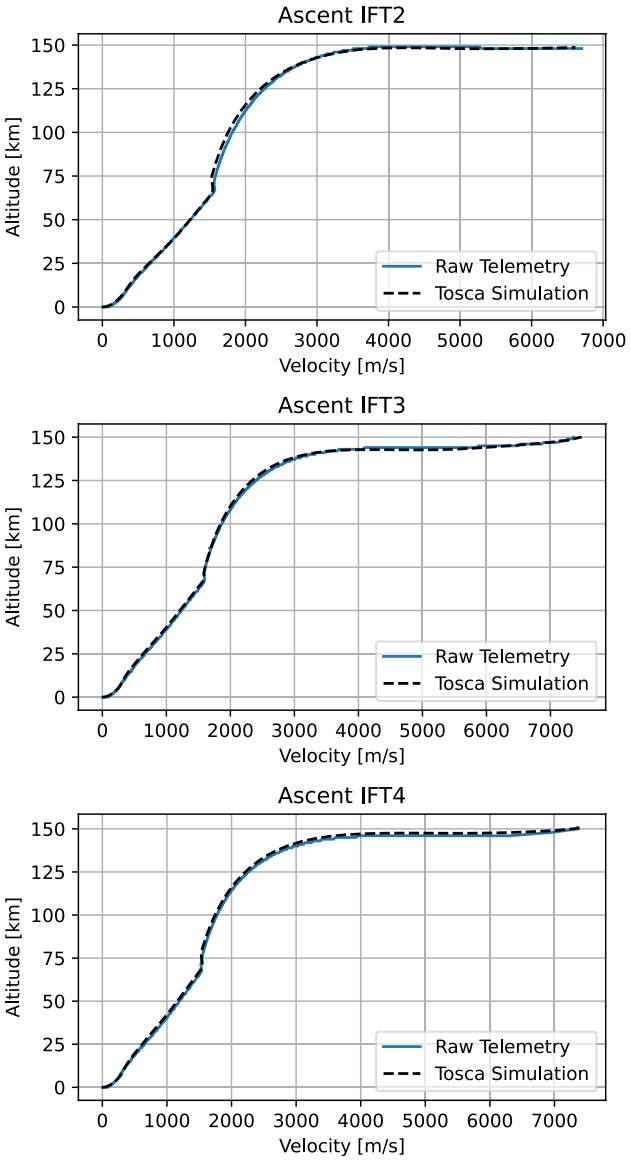


**Fig. 10** Starship's altitude over velocity from telemetry and the Tosca simulation for IFT 2, IFT3, and IFT4

pitching downrange and the thrust is gradually reduced to limit the aerodynamic loads. The point of maximum dynamic pressure (Max Q) is reached between 55 and 70 s. Following MaxQ, the thrust is increased again and plateaus around 80% of its initial value. Approaching stage separation, the thrust is gradually cut back to 60%. A representation of this profile is shown by the massflow in Fig. 15.

Around 160 s after launch, the first stage's main engine cut-off (MECO) occurs, with all but three booster engines shutting down. Hot staging begins 6–8 s after MECO, with all six upper stage engines igniting and the stages separating approximately 1 s later. This separation occurs at velocities between 1520 m/s and 1590 m/s, and altitudes ranging from

71 km to 74 km. The subsequent descent of the booster is addressed in Chapter 2.2.2.

The Starship's ascent continues with an initial acceleration of approximately 4.5 m/s$^2$, maintaining constant thrust until the maximum acceleration of 35 m/s$^2$ is reached 450 s post-launch. The trajectory levels out at altitudes between 140 km and 150 km. The live broadcast's attitude indicator shows the Starship's nose slightly elevated during this phase, indicating a positive angle of attack (AoA). The second-stage engine cut-off (SECO) occurs in two stages: first, the three vacuum engines are shut down. 10–30 seconds later, the remaining three engines are shut-off. The ascent of IFT-3 and IFT-4 ended with a velocity of 7360 m/s at an altitude of 150 km. IFT-2 ended prematurely 8 min and 6 s after lift-off with an explosion of the Starship at a velocity of 6700 m/s at an altitude of 148 km.

### 2.2.2 Booster return

The telemetry of the Super Heavy's return trajectories for IFT-3 and IFT-4 is shown in Fig. 11 along with the Tosca simulation results. The return trajectory for IFT-2 is omitted due to the booster's explosion shortly after stage separation.

Immediately after stage separation, the booster initiates the boostback maneuver. The booster turns by 150° into a horizontal position with its engines pointing towards its horizontal flight direction. The turn maneuver takes 15 seconds. The second ring of 10 engines is reignited during the turn, increasing the total number of running engines to 13. The booster stays under thrust in its horizontal position until the engines are shut down 1 min after stage separation. During the boostback maneuver, the Super Heavy accelerates back to its launch site, reversing the horizontal velocity while its vertical velocity remains largely unchanged. During IFT-2, the booster changed its horizontal velocity from 1400 m/s away from the launch site to 100 m/s towards the launch site. During IFT-3, even 250 m/s towards the launch site were reached. However, these velocities were insufficient to return to the launch site, resulting in trajectories terminating in the Gulf of Mexico. A successful return to the launch site was conducted during IFT-5 [37] and IFT-7 [38], here vertical velocities of 500 m/s towards the launch site were reached.

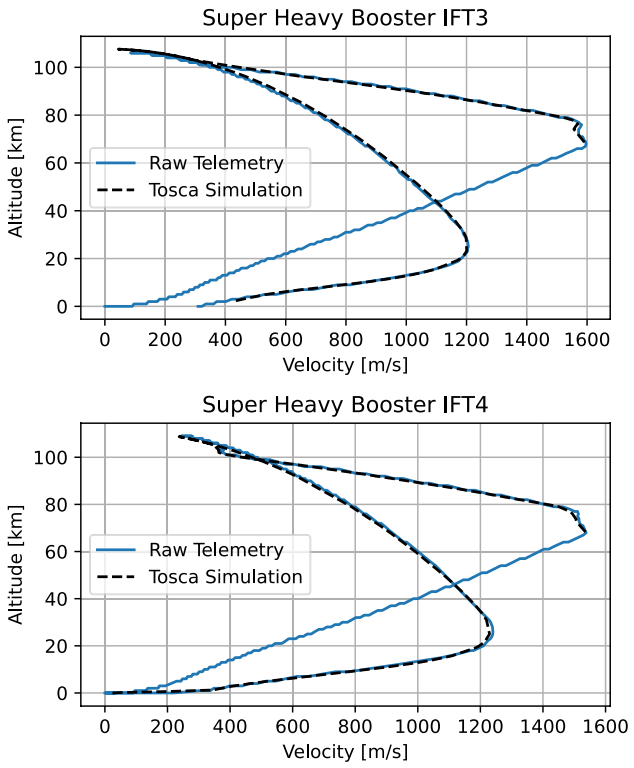


**Fig. 11** The Super Heavy's altitude over velocity from telemetry and the Tosca simulation for IFT3 and IFT4

Following the boostback maneuver, the booster enters a ballistic trajectory, reaching a maximum altitude of 110 km before descending engines first back into the atmosphere. Below 30 km altitude, aerodynamic drag begins to significantly decelerate the booster. In its peak, the aerodynamic deceleration exceeds 50 m/s$^2$, as shown in Fig. 16. The booster hits its maximum velocity during reentry of 1200 m/s for IFT-3 and 1240 m/s for IFT-4 at an altitude of 25 km. Less than 2 km above the surface and still at transonic velocity, the booster relights the 13 inner engines for the final landing burn. It again decelerates with more than 50 m/s$^2$, until at a velocity around 60 m/s all but the the three innermost engines are shut down. The booster then decelerates more gradually and contacts the water at only a few meters per second. The final landing burn was successfully executed during IFT-4, whereas IFT-3 failed to reignite its engines, resulting in a high-velocity impact into the water.

### 2.2.3 Starship reentry

To understand the Starship's reentry dynamics, this study focuses exclusively on the IFT4 since IFT2 concluded during ascent and IFT3 experienced an uncontrolled reentry, resulting in the premature destruction of the Starship. The telemetry velocity and altitude of the IFT4 Starship reentry are shown in Fig. 12, alongside the results of the Tosca remodeling. The shown telemetry starts 44 min and 37 s after lift-off at an altitude 111 km and a velocity of 7411 m/s. The initial ballistic trajectory is matched in the Tosca simulation with an initial flight path angle of −1.05°.

First plasma becomes visible at an altitude of 107 km. Significant aerodynamic forces start to alter the trajectory below 80 km altitude. The trajectory levels out at 68 km and the Starship remains at that altitude for several minutes. The altitude is kept constant by gradually decreasing the Starship's AoA in response to its decreasing velocity.

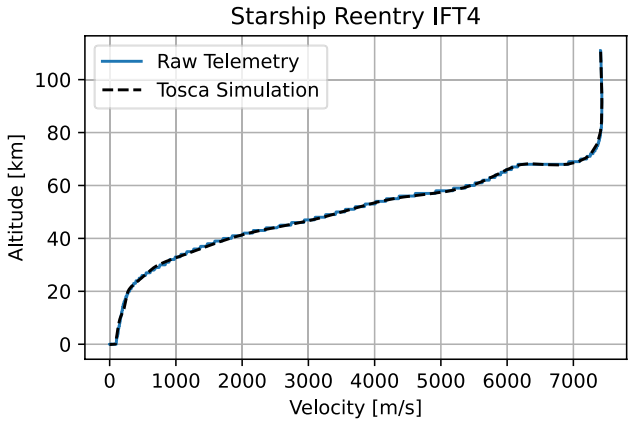


**Fig. 12** The Starship's altitude over velocity from telemetry and the Tosca simulation for the reentry of IFT4

As the initial reentry AoA is larger than the maximum lift AoA, the lift coefficient increases, ensuring that the lift remains constant as the Starship decelerates to 6075 m/s. Afterwards, the Starship's attitude, as observed in the live broadcast, remains largely unchanged as the vessel falls deeper into the atmosphere and decelerates further.

At an altitude of 57 km, visible damage appears on the control surfaces, with heat shield tiles detaching and the reentry plasma beginning to erode the now-exposed frame of the vehicle. Despite the extensive damage to the control surfaces, that accumulates throughout the flight, the Starship successfully maintains attitude control and continues its controlled reentry. The maximum deceleration of 15 m/s$^2$ is reached at an altitude of 30 km. Upon reaching an altitude of 20 km, the Starship transitions to subsonic speeds and alters its flight orientation to the "Skydiver" orientation. This orientation is characterized by a 90° AoA to maximize drag and minimize the terminal velocity.

As the Starship descends below 1 km altitude at a velocity of 100 m/s, it reorients to a 180° AoA and reignites its engines for the final landing burn. The Starship completes a soft landing in the Indian Ocean 1 h, 5 min, and 57 s after lift-off.

## 2.3 Remodeling of the integrated flight tests

Using the models outlined in Chapter 2.1, simulations of IFT2, IFT3, and IFT4 are conducted using the DLR-internal trajectory simulator *Tosca*. The primary objective is to gain a better understanding of the Starship system and to calibrate and validate the existing models for improved accuracy.

### 2.3.1 Ascent remodeling

The basis for the remodeling of the ascent is the flight path angle and acceleration extracted from the publicly available telemetry of all three launches [32, 34, 35]. Since the telemetry itself only provides the total velocity, altitude, and fuel level, additional processing is necessary to derive the needed information. The total acceleration is directly determined from the total velocity, as the change in velocity between two consecutive data points. The resulting acceleration of IFT4's ascent is illustrated in Fig. 13.

To estimate the flight path angle, the vertical velocity is determined from the altitude and then used to calculate the horizontal velocity from the total velocity. Next, the flight path angle is computed using the horizontal and vertical velocities. Figure 14 presents the resulting flight path angle for IFT4. The transmitted altitude is given with the low resolution of 1 km, which leads to unrealistic fluctuations of the

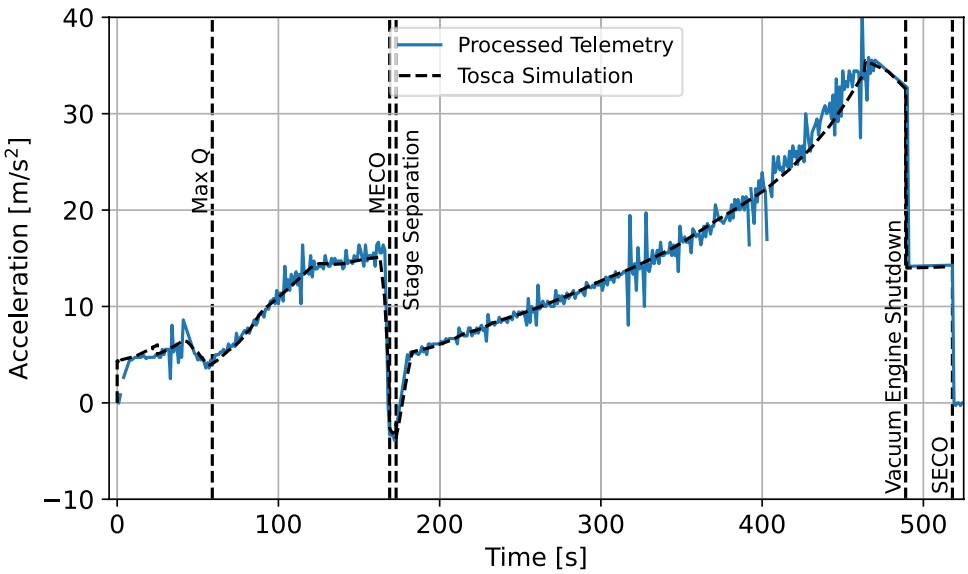


**Fig. 13** Acceleration of Starship's IFT 4 ascent and the simulated trajectory

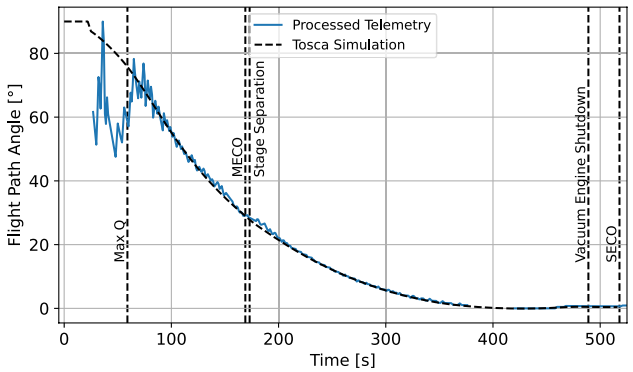


**Fig. 14** Flight path angle of Starship's IFT 4 ascent and the simulated trajectory

derived vertical velocity throughout the early phase of the flight.

To simulate the test flights, the initial relative fuel levels from the telemetry of the Starship and Super Heavy are matched. In addition, the timing of significant events throughout the flight is replicated in the simulation. Throughout the simulated flight, the engine throttling, the initial pitch rate, and the AoA are adjusted to closely match the acceleration and flight path angle of the real flight. The achieved match for IFT4 is presented in Figs. 13 and 14.

The input parameters are not adjusted arbitrarily; rather, adjustments were made only when supported by secondary indicators. This approach is essential for achieving the most accurate model of the system. Due to the limited publicly available information about the Starship and Super Heavy, the simulation model is highly underdetermined. The telemetry data could be reproduced by countless combinations of input parameters, thus necessitating the use of multiple indicators for setting or adjusting parameters.

For instance, the ascent of the first stage shows no indication for a change in AoA; therefore, the simulated AoA remains at 0° throughout the first stage's ascent. However, the fuel telemetry shown in Fig. 15 indicates throttling of the first stage's engines. Accordingly, throttling is applied in the simulation to match the acceleration profile of the test flights.

To achieve this close of a match with the telemetry data, a few adjustments to the initial model were necessary. One key deviation was the initial TWR of the Super Heavy. The telemetry indicates a TWR around 1.4 immediately after launch for IFT2, IFT3 and IFT4. However, assuming 33 Raptor 2 engines operating at 250 bar main combustion chamber pressure (MCCP) (see Table 1), the model only achieves a TWR around 1.2.

In addition, inconsistencies in the mass flow rate were observed. The mass flow rate was calculated from the telemetry fuel level with the assumption that 100% fuel level equals 3300 t of fuel for the Super Heavy and 1200 t for the Starship. As depicted in Fig. 15, the mass flow after Max Q and during the Starship's ascent is accurately modeled by the

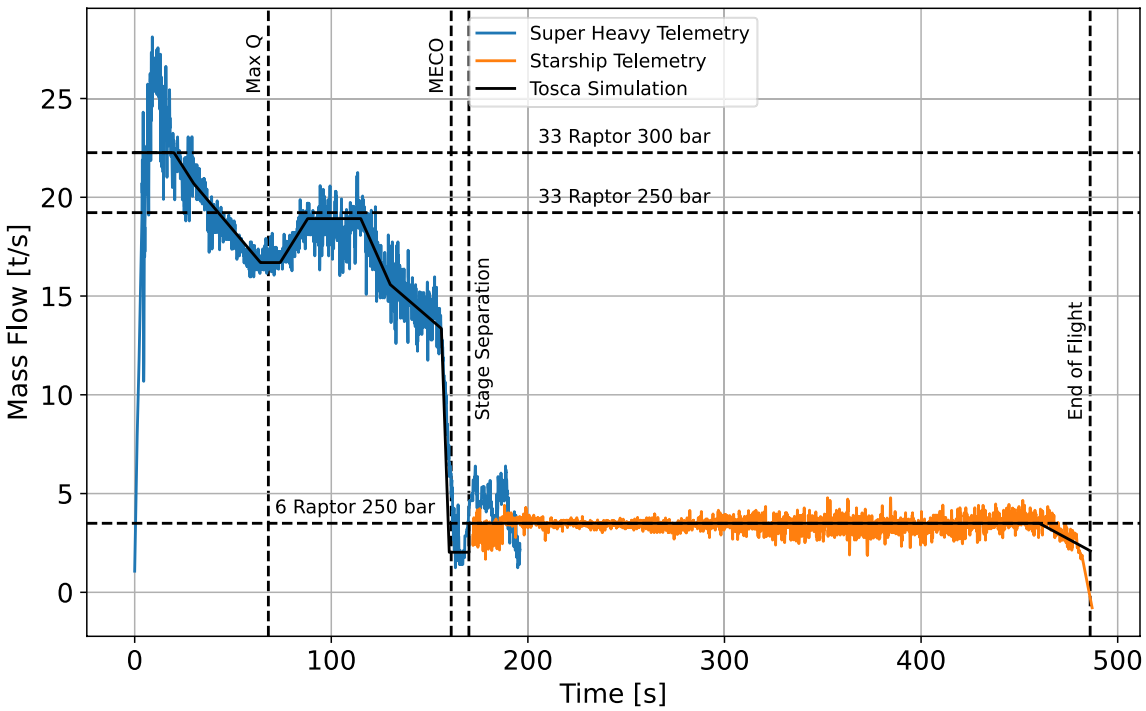


**Fig. 15** Comparison between the mass flows during Starship's IFT 2 and the simulated trajectory

Raptor 2 model at 250 bar MCCP. However, a higher mass flow rate was observed during the early flight, indicating a higher MCCP at that stage. A good fit for the initial TWR of 1.4 is achieved for a MCCP of 300 bar. Despite this, the early mass flow still spikes above the mass flow predicted for 33 Raptor 2 at 300 bar MCCP. The realism of this initial spike is uncertain, as it could be influenced by sensor inertia, and no corresponding spike is observed in the acceleration data in Fig. 13.

These findings suggest that the Super Heavy's Raptor engines initially run at MCCPs higher than 250 bar, potentially approaching SpaceX's goal [19] of operating the Raptor 2 at 300 bar outside the test stand. However, it appears that the engines are still limited to operating at MCCPs around 300 bar for a restricted duration. For instance, the Super Heavy does not return to MCCPs above 250 bar after throttling the engines around Max Q, and the Starship's engines appear to run at 250 bar MCCP throughout the flight.

The approach outlined here enabled a detailed and accurate simulation of the Super Heavy's and Starship's behavior and trajectory. This is evidenced by the strong correlation between the real and simulated trajectories, as shown in Figs. 10, 13, and 14.

### 2.3.2 Booster return remodeling

The reentry of the Super Heavy for IFT3 and IFT4 is remodeled analogous to the ascent's remodeling procedure. The simulation starts at stage separation. The initial velocity, altitude, flight path angle and relative fuel level are matched to the telemetry state at stage separation. Key events, such as the start and end of the boostback and landing burns, are precisely synchronized between the simulation and the actual flight data. To accurately model the trajectories, the acceleration and flight path angle are again closely aligned with the observed data throughout the flight by adjusting the AoA and engine throttling of the Super Heavy. The resulting acceleration and flight path angle curves for IFT4 and the corresponding Tosca simulation are shown in Figs. 16 and 17.

A critical aspect of accurately modeling the complex boostback burn was the precise representation of the booster's orientation and the number of active engines during the maneuver, as described in Chapter 2.2.2. The simulation employs a detailed AoA and throttling profile to replicate this, thereby closely matching the observed irregular acceleration curve of the boostback.

To simulate the large aerodynamic breaking shortly before the landing burn, the simulated booster is flown with a high AoA of 25°. The live broadcasts of later test flights [37, 38] clearly show the presence of an AoA, but do not enable a deduction of the angles size. Therefore, the necessary large angles could indicate an underestimation of the booster's aerodynamic drag during its super- and transonic flight. At an altitude of 10 km, the simulation reaches the maximum dynamic pressure of 150.000 Pa during this breaking phase. In the later simulations, the booster return trajectories will be constrained to dynamic pressures below 150.000 Pa.

Towards the end of the flight, at lower velocities, the flight path angle calculated from the telemetry again shows high noise and faulty results due to the low altitude resolution.

Again, a detailed and accurate simulation of the test flights is achieved. The velocity and altitude throughout the trajectory of both test flights are closely matched by the simulation, as illustrated in Fig. 11.

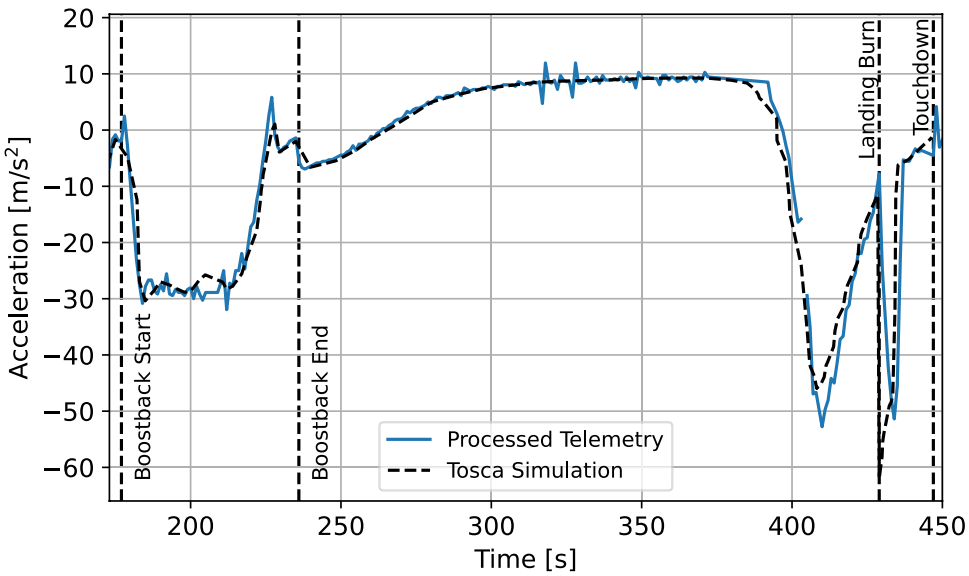


**Fig. 16** Acceleration for Super Heavy's IFT 4 reentry and the simulated trajectory

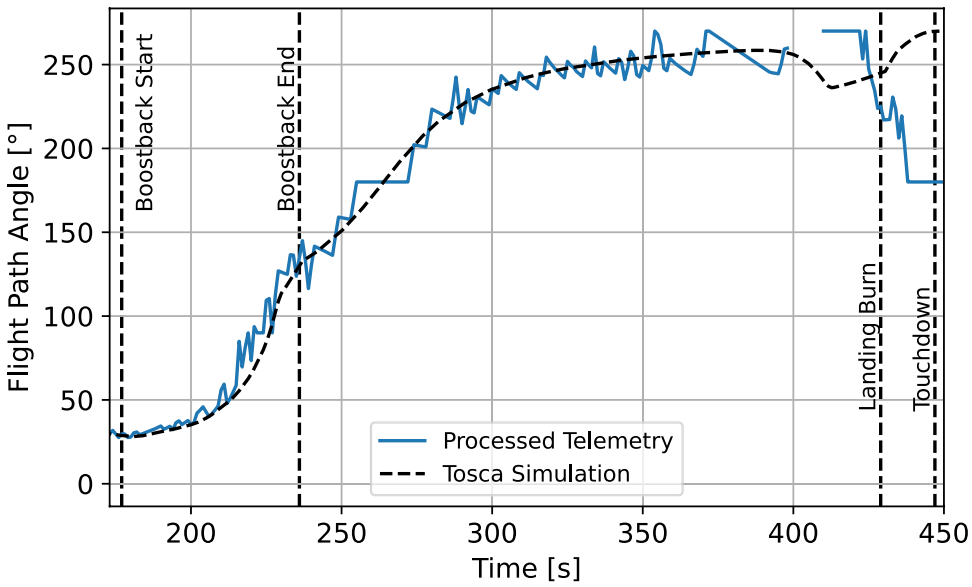


**Fig. 17** Flight path angle for Super Heavy's IFT 4 reentry and the simulated trajectory

#### 2.3.3 Starship reentry remodeling

To remodel the Starship's reentry during IFT4, a third Tosca model is implemented. The model starts at an altitude of 111 km, a velocity of 7411 m/s and a flight path angle of −1.05°. An AoA profile is utilized to control the vehicle throughout the flight. This profile aims to match the attitude changes observed during IFT4, as described in Chapter 2.2. Initially, the vehicle enters with a constant AoA, which is gradually decreased during the leveling out of the trajectory at 68 km altitude and afterward kept constant until the Starship enters its "skydiver" orientation around an altitude of 20 km. Due to the lack of precise AoA data from the broadcast, multiple angle configurations are tested to find the best fit. The closest match between the simulated and real flight is obtained for an initial AoA of 70°, which is then lowered to 55°. The corresponding altitude and velocity profile is shown in Fig. 12. Below 20 km, the AoA is set to 90°, to represent the "skydiver" orientation. The vessel retains this orientation until seconds before the landing, the AoA is increased to 180°, and the three central Raptor engines are relit for the landing burn.

In conclusion, the simulation accurately captures the dynamics of the Starship's reentry during IFT4. As shown in Fig. 12, the velocity and altitude profiles of the simulated trajectory align closely with the actual flight data.

### 2.4 Payload performance

In the following chapter, the models described in Chapter 2.1 and calibrated in Chapter 2.3 are used to extrapolate the Starship's payload-to-orbit performance for fully reusable operations. The Starship's behavior during the suborbital test flights, detailed in Chapter 2.2 is adjusted to reflect the future operational state. The ascent trajectory is modified from suborbital to orbital and the return trajectory is adapted to ensure the Super Heavy's return to the launch site. Key features of the Starship's behavior during the test flights are closely replicated. These features include the hot-staging maneuver, the throttling around Max-Q, the maximum acceleration of the Starship and Super Heavy, or the return of the booster without reentry burn. Two configurations are investigated: the current Starship V1 and the enlarged Starship V2. The adapted model of Starship V2 and Super Heavy V2 is described in Chapter 2.4.2. The maximum possible payload is estimated for the direct ascent into a 250 × 300 km orbit with an inclination of 26° from the SpaceX's Boca Chica facility in Texas, located at 25.996°N, 97.155°W. The orbit represents a potential staging orbit for a translunar trajectory. Compared to the target orbit of the later investigated RLV C5 (see Chapter 3), the Boca Chica launch site causes a 1° higher inclination.

#### 2.4.1 Payload performance of starship V1

The Starship V1 configuration represents the current IFT4 Starship and directly utilizes the models employed for the remodeling of the test flights. A maximum fuel load of 3300 t for the first and 1200 t for the second stage is assumed.

The ascent and booster return trajectories are simulated as described in Ref. [8]. The Δv required for the Boostback is dominated by the need to neutralize the horizontal velocity away from the launch site; therefore, it is beneficial for the Boostback to have the stage separation at a higher flight path angle. In contrast, the ascent's goal is to generate horizontal velocity to achieve the desired orbit, thus it benefits from a lower flight path angle at stage separation.

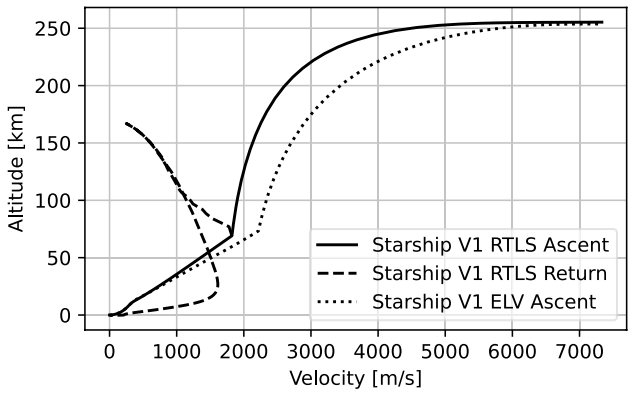


**Fig. 18** Altitude over velocity for the ascent and booster return trajectories of the Starship V1 simulation

Overall, this compromise causes a slightly steeper ascent compared to an expendable ascent of the same vehicle, as shown in Fig. 18. The final return to launch site (RTLS) trajectory uses 265 t of fuel for the return of the booster. In addition, considering the reserve and residual fuel, 3006 t of fuel are used for the booster's ascent. It is assumed that the booster's Raptor engines return to maximum thrust after the throttling around Max-Q.

The Starship also needs to reserve fuel for its deorbit maneuver and landing burn. Unlike the booster, no iterative process is needed to determine the return fuel for the Starship, as it consistently returns from the same orbit and with the same mass, assuming a return without payload. For the deorbit maneuver and the landing burn of the Starship, 20 t of fuel are reserved, with an additional 36 t for reserves and residuals. This leaves a total of 1,144 t of fuel available for the second stage's ascent.

The altitude and velocity profiles of the Starship V1's ascent and booster return are depicted in Fig. 18. The trajectory closely resembles the test flight trajectories, shown in Figs. 10 and 11. The higher target orbit necessitates a steeper trajectory. Furthermore, the return of the booster's MCCP to 300 bar after Max-Q moves the stage separation to a lower altitude of 68 km and higher velocity of 1826 m/s. The Super Heavy's boostback burn is extended and the return trajectory reaches a higher maximum altitude of 163 km.

An expendable ascent is also investigated and shown in Fig. 18. For this ascent, no fuel is reserved for the return of the booster or the descent of the Starship, freeing 260 t of fuel in the booster and 20 t in the Starship. The trajectory is directly optimized by TOSCA.

With the shown trajectory and described model of the fully reusable Starship V1 configuration, the simulation achieves a payload to LEO of 59 t. This puts its payload capabilities close to the 63.8 t [39], the Falcon Heavy achieves without recovering any boosters. 30 t A completely expendable ascent of the Starship configuration increases the achievable payload to 132 t.

IFT4 did not include any subsystems for housing or deploying payloads. Therefore, the Starship V1 model does not reserve mass for movable payload bay doors or other payload deployment mechanisms. The additional mass needed for such mechanisms is not represented in the calculated payloads. Thus, the final net payload will be lower.

### 2.4.2 Starship V2 model

The Starship V2 configuration is a future upgraded version of SpaceX's reusable launch system, introduced in April 2024 [10]. The presented configurations and their key parameters are shown in Table 4. The Starship V2 is supposed to represent the vehicle in an early operational phase after its current test phase. The key differences to the current test version are a larger fuel load, a slight increase in length, and the use of the more capable Raptor 3 engines. With these changes, SpaceX plans to achieve a payload of 100 t and more. SpaceX also announced an even larger Starship V3 version with a payload capacity beyond 200 t, which will not be investigated in this paper.

To investigate the Starship's early operational performance, a model of the Starship V2 is created. The model is based on the previously described Starship V1 model. The key parameters of the model are shown in Table 5.

The fuel capacity is increased to 3650 t for the first stage and to 1500 t for the second stage. A new PMP model is created to represent the larger tanks, longer fuel lines, and increased fuel flow. The dry mass increases for the Super Heavy by 8 t to 319 t and for the Starship by 8 t to 126 t. Overall, the structural index lowers, as all masses but the tanks and fuel lines are kept constant between Starship V1 and V2 and the larger tanks have a more favorable fuel-to-drymass ratio.

**Table 4** Performance data of current and future Starship versions presented by SpaceX [10]

| | Flight 3 | Starship 2 | Starship 3 |
|---|---|---|---|
| Payload to orbit [t] | N/A | 100+ | 200+ |
| Booster propellant load [t] | 3300 | 3650 | 4050 |
| Ship propellant load [t] | 1200 | 1500 | 2300 |
| Booster lift-off thrust [tf] | 7130 | 8240 | 10,000 |
| Ship initial thrust [tf] | 1250 | 1600 | 2700 |
| Ship sea-level engines | 3 | 3 | 3 |
| Ship vacuum engines | 3 | 3 | 6 |
| Booster height [m] | 71 | 72.3 | 80.2 |
| Ship height [m] | 50.3 | 52.1 | 69.8 |
| Total height [m] | 121.3 | 124.4 | 150 |

**Table 5** Technical parameters of the V2 Starship and Super Heavy models

| | Starship V2 and Super Heavy V2 |
|---|---|
| 1st stage | |
| Propellant mass | 3650 t |
| Dry mass | 319 t |
| Structural index with propulsion | 8.8% |
| Structural index without propulsion | 5.9% |
| Total mass | 3969 t |
| Engine $I_{SP}$, sea level | 329 s |
| Engine $I_{SP}$, vacuum | 348 s |
| Tank volume | 4350 $m^3$ |
| Length | 73 m |
| Fuselage diameter | 9 m |
| 2nd stage | |
| Propellant mass | 1500 t |
| Dry mass | 126 t |
| Structural index with propulsion | 8.4% |
| Structural index without propulsion | 7.0% |
| Total mass | 1626 t |
| Engine $I_{SP}$, vacuum | 366 s |
| Tank volume | 1697 $m^3$ |
| Length | 51 m |
| Fuselage diameter | 9 m |
| Lift-off mass (without payload) | 5595 t |

The Raptor 3 engines are modeled by a raise of the engine's MCCP to 350 bar. This increases the initial thrust of the booster to 81.84 MN and the ship's initial thrust to 1.61 MN. The aerodynamic model is kept constant.

### 2.4.3 Payload performance of starship V2

The model described in Chapter 2.4.2 is used to simulate the performance of the Starship V2 configuration. Although the Super Heavy's dry mass increases, the fuel needed for the return of the booster is reduced to 250 t. The reason behind this decrease are the more efficient Raptor 3 engines and a reduction in the velocity at stage separation. For the Starship, the fuel mass reserved for reentry remains at 20 t.

The altitude and velocity profile, depicted in Fig. 19, shows only minimal differences compared to the profile of the Starship V1 configuration, shown in Fig. 18. The point of stage separation moves to a slightly lower altitude and velocity of 66 km and 1725 m/s, respectively. The relative increase in fuel mass is greater for the Starship, resulting in a smaller share of the total Δv provided by the Super Heavy booster.

In the simulations, the fully reusable Starship V2 configuration achieves a payload to LEO of 115 t. This almost

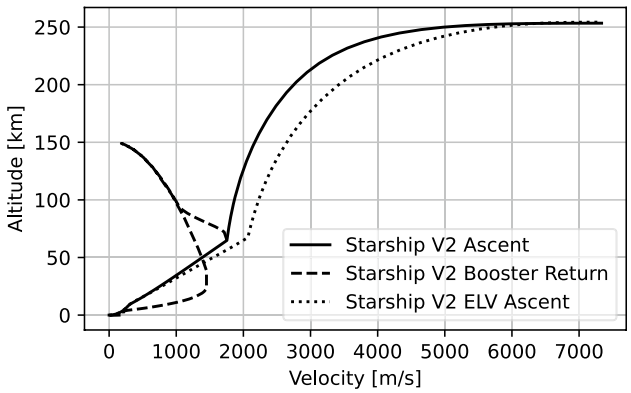


**Fig. 19** Altitude over velocity for the ascent and booster return trajectories of the Starship V2 simulation

doubles the payload capability of the simulated Starship V1 configuration and reaches the announced 100 + t. The proposed expansion of the configuration appears to be a suitable strategy for achieving the intended payload objectives. With this immense capacity, the configuration would surpass the largest currently operational launch system, the expendable Block 1 Space Launch System [40]. If the Raptor 3 engine mass of 1720 kg published by SpaceX [22] is assumed, the payload increases further to 125 t. The expendable ascent of the V2 Starship achieves a payload of 188 t in the simulations, which would surpass the Saturn V's payload capacity [41]. Again, the used model does not include a payload deployment mechanism. The achieved payloads and key masses of both Starship versions are shown in Table 6.

The analysis indicates that while SpaceX's payload objectives are technically feasible, the primary challenge lies in attaining full and rapid reusability. The significant damage sustained by the Starship during IFT-4 [32] highlights that developing a rapid reusable thermal protection system remains a critical obstacle.

**Table 6** Payload and total mass of the V1 and V2 Starship and Super Heavy models

| | Starship V1 and Super Heavy V1 | Starship V2 and Super Heavy V2 |
|---|---|---|
| Propellant mass | 4500t t | 5150 t |
| Total dry mass | 429 t | 445 t |
| Lift-off mass (without payload) | 4931 t | 5596 t |
| Gross fully reusable payload | 59 t* | 115 t* |
| Gross expendable payload | 132 t* | 188 t* |

*No payload deployment mechanism included

## 3 RLV C5

In the face of the enormous potential and fast progress of the Starship configuration, innovative European concepts for the launch of Super Heavy payloads are necessary to be competitive and independent in the international launch market. The following chapter investigates one concept for a partially reusable, super-heavy space transportation system. It employs components currently under investigation as part of the SpaceLiner [5] hypersonic transport family to achieve a payload to LEO beyond 50 t.

### 3.1 Model description

The proposed concept integrates the winged, reusable, multipurpose SpaceLiner booster (SLB) stage and an expendable second stage, aiming to maximize payload capacity. Both stages are propelled by the FFSC SpaceLiner main engine (SLME), utilizing cryogenic liquid hydrogen and liquid oxygen as propellants. This configuration, referred to as "RLV C5," is modeled using the SART numerical tools outlined in 2.1.1. A simplified CAD model of the RLV-C5 is shown in Fig. 20.

A similar configuration was previously examined in 2016 with the SpaceLiner Cargo [42], which paired the SLB with a fully reusable cargo version of the SpaceLiner. It achieved a deployable payload of 26.15 t into an unstable $30 \times 250$km orbit and will serve as a reference of the SpaceLiner's fully reusable capabilities.

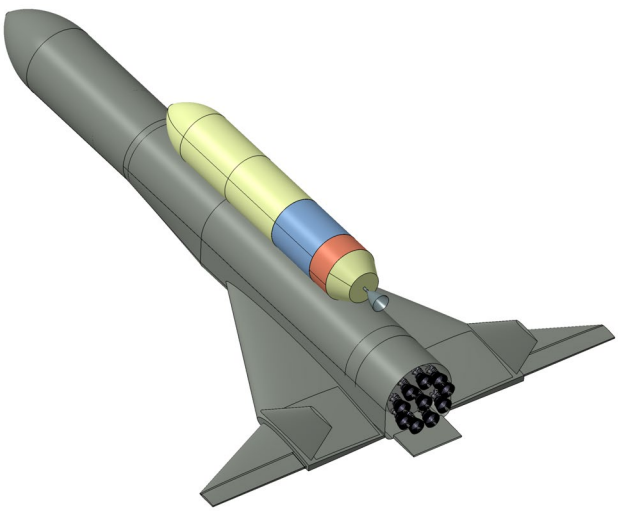

**Fig. 20** Simplified CAD model of the RLV-C5 with the SpaceLiner booster in grey, the second stage's oxygen tank in red, the second stage's hydrogen tank in blue, and the second stage's thruster frame and fairing in yellow

#### 3.1.1 SpaceLiner 8 booster stage

The reusable SpaceLiner booster is a vertical take-off horizontal landing stage, originally proposed in 2005 [43]. Since its inception, the SpaceLiner and its booster stage have undergone several updates and iterations [4, 5, 44, 45]. The used SpaceLiner 8-V3 booster is a model currently under design. A detailed description of the booster and its design process can be found in Refs. [46, 47].

The booster features a conventional tank design with two large integral tanks for LOX and liquid hydrogen (LH2), separated by bulkheads and resembling the space shuttle external tank (ET) [4]. The tanks house a total of 1290 t of propellant. In contrast to the ET, it is equipped with a propulsion system, and wing structures with landing gear. It is fitted with an ogive nose for aerodynamics and housing subsystems. The tanks, with an external diameter of 8.8 m, are load-bearing. The LH2 tank interfaces with the parallel mounted upper stage through an intertank structure. At the root of the wing, a NACA 66–206 section is used, and for the mid-chord, a NACA 2414 foil has been selected to accommodate the outer wing segment. This outer wing segment has a NACA 2408 profile and is housed inside the inner wing during hyper- and supersonic flight. For sub- and transonic flight, it is deployed to enhance the configurations gliding performance. The wings are designed with a classical aircraft differential architecture, incorporating ribs, spars, and stringers. The stage has a total dry mass of 219 t, yielding a structural index of 17%. [46, 47]

The propulsion system consists of ten SpaceLiner main engines (SLME) with an expansion ratio of 33 providing a sea-level thrust of 21 MN. The engines are described in detail in Chapter 3.1.3. The baseline recovery method for the reusable SLB is the in-air capturing (IAC) technique, where a large subsonic aircraft captures and tows the winged vehicle. Extensive simulations and lab-scale experiments demonstrate its viability compared to other recovery methods. [48, 49]

#### 3.1.2 Expendable second stage

The second stage is designed to maximize the configuration's LEO payload capacity. The stage maintains a constant diameter of 6.5 m, with its length adjusted according to the required propellant load. It is equipped with a 24 m long fairing, that provides 700 $m^3$ of internal volume at a mass of 6400 kg. The stage is mounted laterally on the SLB and is powered by a vacuum optimized SLME with a 59 expansion ratio, burning cryogenic LH2 and LOX. Specifications of the engine are provided in Chapter 3.1.3. The engine itself has a mass of 3920 kg and additional 308 kg are allocated to represent the reaction control system engines.

To explore a range of possible fuel loads, the stage's structure mass is estimated by structural index (SI). The SI is calculated by an exponential function based on the ascent propellant. This function is derived from a regression analysis of H2/LOX upper and lower stages [50].

$$SI\left(m_{\mathrm{p}}\right) = 0.279337 \cdot m_{\mathrm{p}}^{-0.188090}$$

This SI accounts for all systems besides the engine, interstage and fairing, which are modeled by constant masses. The resulting masses for all investigated propellant loads are shown in Table 7. Propellant loads from 120 t to 165 t are investigated, resulting in stages with dry masses between 24.5 t and 28.5 t. In addition to the ascent propellant, the stages also include 350 kg of deorbit propellant and 5.6 t of residual and reserve propellant, increasing the total propellant mass of each stage by an additional 6 t.

#### 3.1.3 SpaceLiner main engine

Both stages employ a modified version of the SpaceLiner main engine (SLME) [46]. Similar to the Raptor engine, the SLME operates on a FFSC cycle. However, it combusts cryogenic liquid hydrogen and cryogenic liquid oxygen at a moderate MCCP of 160 bar. The expansion ratios are optimized individually for the SLB and expendable second stage, while the mass flow, turbo-machinery, and combustion chamber remain consistent with the baseline configuration [51]. The booster engine has an expansion ration of 33 and achieves a thrust of 2427 kN in vacuum and 2111 kN at sea level. In contrast, the second-stage engine uses a larger expansion ratio of 59 and provides 2110 kN in vacuum and 1651 kN at sea level. The engine parameters are shown in Table 8 and a comprehensive description of the engine is found in Refs. [52] and [3]. A CAD rendering of the engines is provided in Fig. 21.

**Table 7** Structural index and mass of all investigated RLV C5 expendable upper stages

| Ascent propellant [t] | SI [%] | Structure mass [t] | Total dry mass [t] |
|---|---|---|---|
| 120 | 11.35 | 13.6 | 24.5 |
| 125 | 11.26 | 14.1 | 24.9 |
| 130 | 11.18 | 14.5 | 25.4 |
| 135 | 11.10 | 15.0 | 25.9 |
| 145 | 10.90 | 15.9 | 26.8 |
| 155 | 10.73 | 16.7 | 27.6 |
| 165 | 10.63 | 17.6 | 28.5 |

**Table 8** Engine parameters of the SpaceLiner main engine [52]

| | SLME | SLME extended nozzle |
|---|---|---|
| Mixture ratio | 6.5 | 5.5 |
| Combustion chamber pressure | 160 bar | 160 bar |
| Mass flow rate | 555.0 kg/s | 477 kg/s |
| Expansion ratio | 33 | 59 |
| $I_{SP}$ in vacuum | 433.4 s | 450.6 s |
| $I_{SP}$ at sea level | 386.1 s | 352.6 s |
| Thrust in vacuum per engine | 2427 kN | 2110 kN |
| Thrust at sea level per engine | 2111 kN | 1651 kN |

### 3.2 Performance

In the subsequent chapter, the model outlined in Chapter 3.1 is used to evaluate the payload-to-orbit performance of the RLV C5. The maximum achievable payload is estimated for the direct ascent into a 250 × 300 km orbit with an inclination of 25° from the Guiana Space Centre in Kourou, French Guiana, situated at 5.24° N, 52.77° W. Again, the DLR-internal trajectory simulation tool TOSCA is used.

#### 3.2.1 Trajectory

The trajectories of the four investigated configurations exhibit large similarities, allowing them to be described collectively. As an illustrative example, the trajectory of the configuration with the 135 t upper stage is shown in Fig. 22.

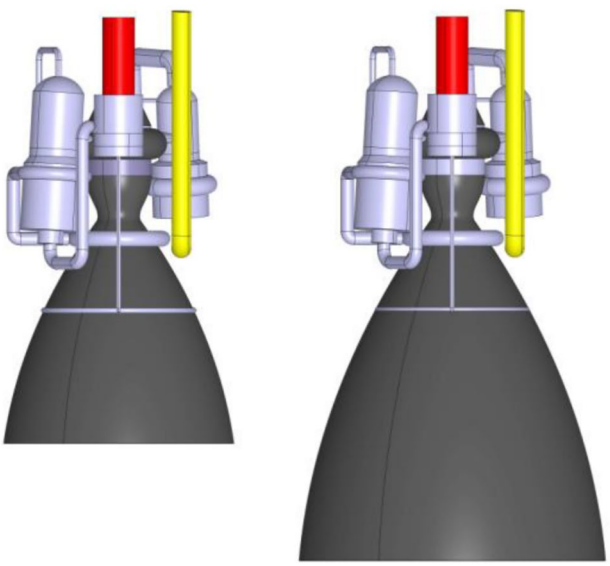

**Fig. 21** SpaceLiner main engine's simplified CAD geometry with nozzle expansion ratio 33 (left) and 59 (right) [52]

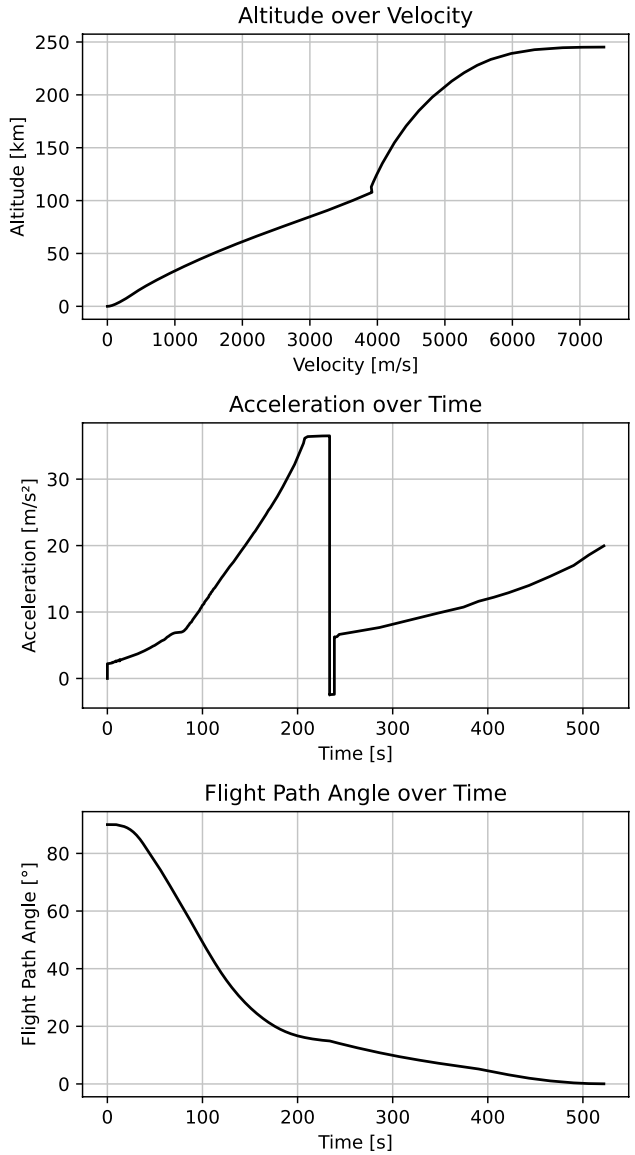


**Fig. 22** Ascent trajectory of the RLV C5 with a 135t upper stage

The vehicle launches with an initial acceleration slightly above 1.2 g. It ascends vertically for the first 9 s to clear the launch tower and afterwards starts to pitch downrange. Throughout the ascent, the vehicle's angle of attack is controlled, while the engines remain at their maximum thrust as long as the acceleration limit is not reached. The MaxQ of 24500 Pa is encountered 84 s after launch at an altitude of 12 km. 210 s after launch and shortly before stage separation, the RLV C5 reaches its acceleration limit of 35 m/s$^2$, prompting a throttle back to maintain a constant acceleration. The first stage's fuel is exhausted 233 s after launch and the stages are separated at low flight path angles < 20°.

The stage separation velocity and altitude differ slightly between the configurations. For the configuration with the largest 135 t upper stage, the separation occurs at 3919 m/s and 107 km and for the configuration with the lightest 120 t upper stage at 4038 m/s and 118 km. The other configurations fall within this range, with heavier upper stages resulting in slower velocities and lower altitudes at separation.

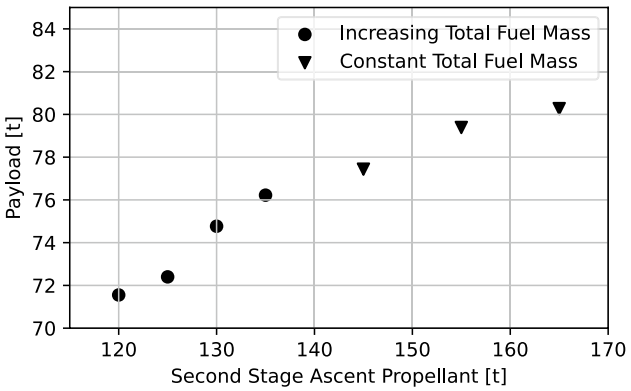


**Fig. 23** Payload to LEO over the second stage's ascent propellant for the RLV C5

Five seconds after separation, the second stage engine ignites and continues the ascent with an initial acceleration of 10 m/s$^2$. Only a few seconds after engine ignition, the fairing is jettisoned. The stage accelerates for roughly 300 s until the final 250 × 300 km orbit is achieved. The SLB's descent trajectory does not impact the payload performance, as no fuel is necessary for the IAC maneuver. The complex maneuver itself is described in detail in Ref. [49].

### 3.2.2 Payload performance

All RLV C5 configurations investigated in this study achieve payloads exceeding 70 t, thereby meeting the initial requirement for launching super-heavy payloads of over 50 t. Two scenarios are examined to evaluate how the second-stage propellant load affects performance: first, a case where the total vehicle propellant mass increases with added second-stage fuel; and second, a case where the total fuel mass is held constant by reducing the first stage's fuel accordingly. These two approaches are analyzed sequentially in the following paragraphs.

In the first scenario, the fuel load of the second stage is increased, while the SLB remains unchanged and is kept at full fuel capacity. Figure 23 illustrates how the payload grows as more propellant is added to the second stage. The trend appears approximately linear within the range analyzed; however, this relationship is likely to tail off at higher fuel loads. Specifically, in the analyzed range, an increase of 5 t in second-stage propellant results in an average payload gain of 1.6 t, with a maximum payload of 76.2 t reached at 135 t of ascent propellant. As shown in Fig. 24, the initial acceleration decreases with increasing upper stage mass. For this study, a minimum initial acceleration of 1.22 g was

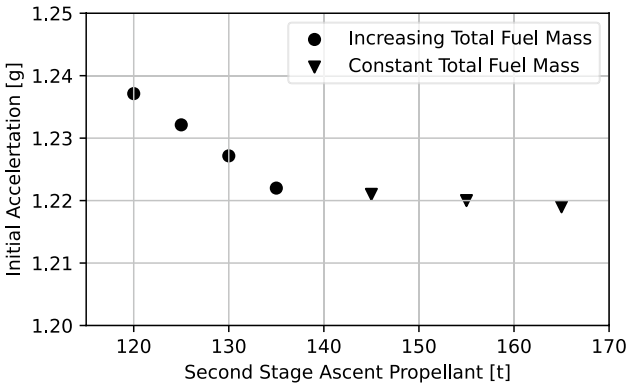


**Fig. 24** Initial acceleration after launch over the second stage's ascent propellant for the RLV C5

established; falling below this threshold causes instability in the implementation of the payload optimization, resulting in non-viable trajectories. Consequently, the available lift-off thrust of the SLB constrains the gross lift-off weight (GLOW), and 135 t marks the practical limit for the upper stage propellant in this scenario.

The second scenario investigates whether payload performance can be improved beyond 76.2 t by redistributing fuel mass instead of increasing it. In this case, every additional kilogram of second-stage fuel is subtracted from the first stage's fuel mass, keeping the total fuel load constant. The first stage remains structurally unchanged, but is not filled to its full fuel capacity. This strategy minimizes increases in GLOW to the additional structure mass that is needed to house the fuel in the upper stage and preserves initial acceleration, as also shown in Fig. 24. Despite the constant fuel mass, staging becomes more optimal, leading to increased payloads. Figure 23 shows that the trend begins to flatten, with the highest payload of 80.2 t reached at a second-stage propellant load of 165 t. However, achieving these additional 4 t of payload requires a significantly enlarged expendable upper stage and leaves some of the SLB's propellant capacity unused. As a result, this solution is less attractive in terms of mass efficiency and cost, unless a substantially larger payload benefit can be realized.

Overall the study yields an optimal upper stage propellant load of 135 t. With that upper stage, the RLV C5 achieves a payload of 76.2 t to the 250 × 300 km target orbit, surpassing the aforementioned theoretical 63.8 t of the expendable Falcon Heavy [39]. The key parameters of the optimal configuration are shown in Table 9.

Compared to the SpaceLiner Cargo's 26 t of payload [31], the RLV-C5 more than doubles the payload capacity and is able to transport the payload directly into a stable orbit. It further expands the mission envelope of the SpaceLiner family. This suggests that the SpaceLiner-based architecture could be extended toward a super-heavy-lift configuration.

**Table 9** Comparison of key parameters of the RLV C5 and the Starship V2 and Super Heavy V2 models

| | RLV C5 | Starship V2 and Super Heavy V2 |
|---|---|---|
| 1st stage | | |
| Propellant mass | 1290 t | 3650 t |
| Dry mass | 219 t | 319 t |
| Structural index with propulsion | 17.0% | 8.8% |
| Structural index without propulsion | 14.3% | 5.9% |
| Total mass | 1509 t | 3969 t |
| Engine $I_{SP}$, sea level | 386 s | 329 s |
| Engine $I_{SP}$, vacuum | 433 s | 348 s |
| Return method | IAC | RTLS |
| Stage mass at MECO | 228 t | 559 t |
| Ascent fuel mass fraction | 84.9% | 84.8% |
| Length | 83 m | 73 m |
| Fuselage diameter | 8.8 m | 9 m |
| 2nd stage | | |
| Propellant mass | 141 t | 1500 t |
| Dry mass | 26 t | 126 t |
| Structural index with propulsion | 18.3% | 8.4% |
| Structural index without propulsion | 15.6% | 7.0% |
| Total mass | 167 t | 1626 t |
| Engine $I_{SP}$, vacuum | 451 s | 366 s |
| Length | 65.6 m | 51 m |
| Fuselage diameter | 6.5 m | 9 m |
| Total length | 82.3 m | 124 m |
| Total mass | 1752 t | 5670 t |
| Total mass to orbit | 102 t | 297 t |
| Reference payload | 76 t | 115 t* |

*No payload deployment mechanism included

Moreover, within the SpaceLiner framework, this configuration could serve as an intermediate step towards the fully reusable SpaceLiner Cargo system, requiring only the relatively straightforward development of a cryogenic upper stage.

## 4 Comparison

The following chapter provides a comparative analysis of the performance and key features of the Starship configuration and the RLV C5. For this comparison, the Starship V2 configuration is used, representing the projected operational state of the system. The key parameters of both vehicles are outlined in Table 9. All references to the mass and performance of the Starship configuration in this chapter are based on the results obtained from the analyses conducted in this paper, rather than relying on SpaceX's publicly stated figures. For each stage i, the structural index with propulsion

$SI_{\mathrm{i}}$ is calculated from the total stage lift-off mass $TLOM_{\mathrm{i}}$ and the total propellant mass $m_{\mathrm{ptot\,i}}$:

$$SI_{\mathrm{i}} = \frac{TLOM_{\mathrm{i}} - m_{\mathrm{ptot\,i}}}{MTOL_{\mathrm{i}}}$$

For the structural index without propulsion $SI_{\mathrm{noprop\,i}}$, the mass of the propulsion system $m_{\mathrm{prop\,i}}$ is subtracted from the numerator.

$$SI_{\mathrm{noprop\,i}} = \frac{TLOM_{\mathrm{i}} - m_{\mathrm{ptot\,i}} - m_{\mathrm{prop\,i}}}{TLOM_{\mathrm{i}}}$$

$m_{\mathrm{prop}}$ includes all masses of the propulsion system, namely the engines, fuel lines, RCS engines, and hydraulics. The ascent fuel mass fraction is calculated from the first stage's total lift of mass $TLOM_1$ and the stage mass at MECO $m_{\mathrm{MECO}}$ :

$$\frac{TLOM_1 - m_{\mathrm{MECO}}}{TLOM_1}$$

It is important to acknowledge that Europe is exploring other reusable launch system architectures, particularly vertical take-off, vertical landing (VTVL) systems. These include ongoing activities under programs such as Themis [53], Callisto [54], and others [55]. While these VTVL concepts are currently focused on small- to medium-lift capabilities, they align more directly with Starship in terms of landing architecture. The winged, partially reusable, hydrogen-fueled RLV-C5 is deliberately chosen for the following comparison to contrast two fundamentally different configurations. The goal is to illustrate the wide range of possible reusable super-heavy launcher architectures and to highlight the system-level implications of key design decisions such as propellant choice and reusability strategy. A more direct comparison study of fully reusable super-heavy launch systems with varying reuse strategies and fuel combinations similar to the ENTRAIN study [56] is currently in work at the DLR SART department.

Although the RLV C5 can launch approximately two-thirds of the payload mass of the Starship V2, the two vehicles operate on vastly different scales. With its gross lift-off mass of 5595 t at launch, the Starship V2 configuration is more than three times heavier than the RLV C5. Several factors contribute to this difference in scale. One significant reason is the large mass of the Starship itself. Considering the dry mass, the return fuel, the residuals, and the maximum payload, the Starship configuration transports 297 t to orbit. Only about 40% of that mass are payload. Another 20% are directly connected to the reusability of the vehicle, this includes the fuel reserved for reentry and landing, the thermal protection system, and the wings. The remaining 40% are the general elements of the vehicle, like its hull, engines, tanks, and the fuel reserves and residuals. Notably, depending on the mission, the Starship itself could be considered part of the payload. It is planned to be refuellable in orbit for extended missions to the Moon or Mars, thereby serving a dual role as both a second stage and an interplanetary vehicle. In contrast, the RLV C5 transports only 102 t into orbit, 74% of that being the payload.

Another factor contributing to the larger mass of the Starship configuration is the lower $I_{SP}$ of the LCH4/LOX burning Raptor engines compared to the LH2/LOX burning SLME. Especially the vacuum $I_{SP}$ is up to 30% higher for the hydrogen engines, which reduces the necessary fuel mass fraction and contributes to a more efficient design.

The total reusability of the Starship also enlarges the configuration considerably. In the current state, the systems and fuel needed for the reusability already take up 20% of the total mass to orbit. This fraction might increase further, as IFT-4 [35] demonstrated that the current thermal protection system has to be reinforced. In contrast, the expendable nature of the RLV-C5 upper stage enables it to achieve a dry mass that is five times lower than that of the Starship. A contributing factor to this reduced dry mass is the early jettisoning of the 6.4 t fairing.

Interestingly, as shown in Fig. 25, the sizes of the first stages of both systems are close, despite the three times larger fuel mass of the Super Heavy. The SLB is with its 83 m a bit longer than the 73 m long Super Heavy but also uses a slightly smaller fuselage diameter of 8.8 m instead of 9 m. The higher density of LCH4 allows the Super Heavy to accommodate a significantly larger fuel load within a comparable volume.

When comparing the ascent trajectories, as depicted in Fig. 26, the primary difference between the RLV-C5 and Starship V1 lies in the staging. The RLV-C5's stage separation occurs later in the flight at more than twice the altitude and velocity. Consequently, a significantly larger portion of the total Δv is provided by the SLB stage than by the Super Heavy booster stage. These differing staging strategies are influenced by their respective recovery methods. The vertical landing RTLS recovery of the Starship's Super Heavy moves the optimal stage separation to lower velocities, as lower velocities require a smaller Boostback maneuver. In contrast, the IAC recovery method used by the SLB eliminates the need for a Boostback maneuver, allowing for higher staging velocities. A second factor behind the large Δv budget of the Starship itself could be its dual role as an interplanetary vehicle. To fulfill this role, it has to provide a large Δv for the interplanetary maneuvers. In its LEO use case investigated in this paper, this shifts the staging to an early stage separation. Furthermore, on the SLB's side, as described in Chapter 3.2, the initial thrust limits the size of the second stage, which constrains the possible Δv budget of the second stage.

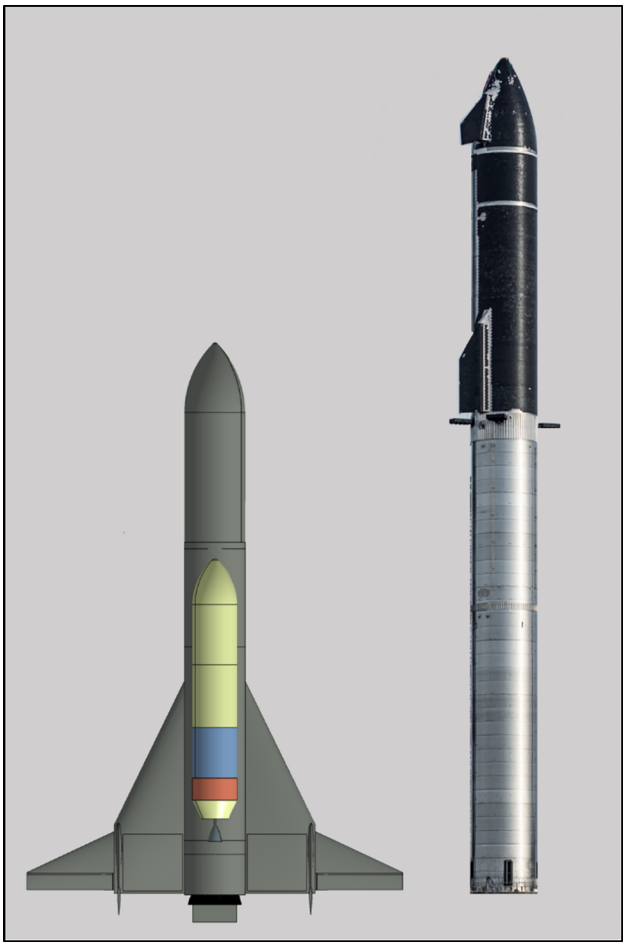

**Fig. 25** Size comparison between the RLV-C5 and the V1 Starship configuration CC BY-NC 2.0. Source: SpaceX [6]

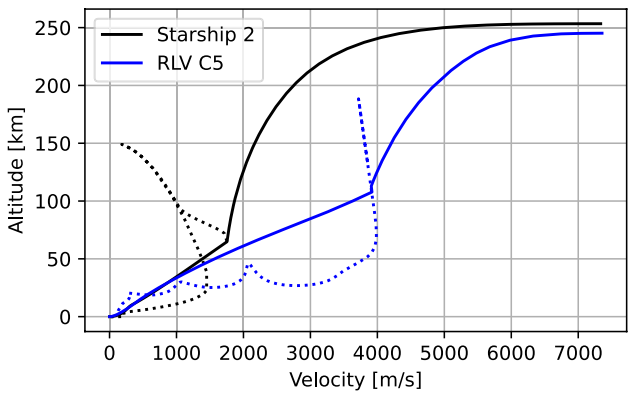


**Fig. 26** Comparison of altitude over velocity diagram for the ascent and booster descent trajectories of the Starship V2 in black and the RLV C5 in blue. The ascents are shown as full lines and the booster descents as dotted lines

As shown in Table 9, the Super Heavy has a significantly lower SI than the SLB, primarily due to its larger fuel load, the higher density of LCH4, and the additional structural requirements of the SLB, such as wings. Nonetheless, the fraction of the total mass that is usable as ascent fuel is with ~ 85% almost identical for both configurations, as the Super Heavy has to reserve fuel for the boostback and landing burns. As discussed in Chapter 2.4.1, the Super Heavy has to fly a steeper, less optimal ascent trajectory, to reduce the fuel needed for the booster return. This increases the gravity losses during the ascent. The RLV C5, on the other hand, flies a shallow trajectory to reduce the flight path angle at stage separation and to limit the heat loads during reentry [42]. While the RLV C5 has larger drag losses due to its wings and its shallower trajectory, it ultimately flies a more efficient ascent by minimizing the larger gravity losses.

The comparison shows that competitive payloads in the super-heavy range are achievable with the smaller and lighter RLV C5, as its partially reusable approach allows for an efficient and light upper stage. This vehicle could significantly expand the capabilities of the SpaceLiner family of launch and transport vehicles with minimal additional costs in development. This would add the super heavy launch capability to the European portfolio, without the development costs of a full reusable system. Especially in a scenario with only a few yearly European payloads above 50 t, this could be an efficient option. While the Starship configuration can deliver significantly more mass to orbit, much of that mass is the Starship itself. This is advantageous for missions where the Starship serves as the payload, but it poses a disadvantage for transporting other payloads. The planned rapid turnaround times and large number of reuses of the Starship system may mitigate this drawback, by allowing several launches a week with a relatively low number of vehicles. If the planned high number of reuses and the short turnaround times of the Starship can be achieved cannot be assessed yet.

The different technological readiness levels of both configurations also have to be noted. Where the Starship is already flying in a prototype state, the RLV-C5 and many of its components remain on the drawing board. Nonetheless, the RLV C5 presents an option for Europe to incorporate a super-heavy launch vehicle into its future spaceflight and space transport strategy. The role of the RLV-C5 and other alternatives in a potential European space flight strategy is discussed further in Ref. [57].

## 5 Conclusion

This paper has presented a comparative analysis of SpaceX's Starship and a potential European heavy-lift launch system based on the SpaceLiner concept. The analysis and

remodeling in Chapter 2 highlighted the advancements of the Starship system, particularly in engine performance, mass optimization, and full reusability. With its prognosed ability to carry payloads beyond 100 t to LEO, Starship V2 stands poised to transform global space transport, if it can achieve its goal of rapid full reusability.

In Chapter 3, the paper explored the RLV C5, a European alternative that combines a reusable winged first stage with an expendable upper stage. This design, capable of launching over 70 tons into LEO, integrates a Super Heavy launcher into the SpaceLiner hypersonic transport family. While the Starship's capabilities are unmatched, the RLV C5, with its partially reusable architecture, provides a viable and efficient path forward to European heavy-lift capabilities, with many advantages compared to expendable heavy-lift vehicles.

The comparison of Starship V2 and RLV C5 in Chapter 4 highlights their distinct design approaches. Starship prioritizes full reusability and high payload capacity but carries significant structural mass, while the lighter RLV C5 achieves efficiency with a partially reusable upper stage and hydrogen-fueled engines. The differences reflect trade-offs between reusability and performance. While Starship's rapid turnaround combined with its immense payload may revolutionize large-scale space transport, the RLV C5 offers an effective path for Europe to independently develop partially reusable super-heavy launch capabilities.

**Author contributions** M.H. wrote the main manuscript text and did the technical analysis of the Starship. L.B. did the technical analysis of the RLV C5. M.S. did the technical analysis of the Starship's engines and wrote the Sect. 2.1.1. J.W. supported and advised the technical analysis of the Starship and provided many of the used tools and models All authors reviewed the manuscript.

**Funding** Open Access funding enabled and organized by Projekt DEAL.

**Data availability** No datasets were generated or analyzed during the current study.

## Declarations

**Conflict of interest** The authors declare no competing interests.

**Content to publication** During the preparation of this work, the authors used ChatGPT 4 to revise the text. After using this tool/service, the authors reviewed and edited the content as needed and take full responsibility for the content of the publication.

**Open Access** This article is licensed under a Creative Commons Attribution 4.0 International License, which permits use, sharing, adaptation, distribution and reproduction in any medium or format, as long as you give appropriate credit to the original author(s) and the source, provide a link to the Creative Commons licence, and indicate if changes were made. The images or other third party material in this article are included in the article's Creative Commons licence, unless indicated otherwise in a credit line to the material. If material is not included in the article's Creative Commons licence and your intended use is not permitted by statutory regulation or exceeds the permitted use, you will need to obtain permission directly from the copyright holder. To view a copy of this licence, visit http://creativecommons.org/licenses/by/4.0/.

## References

1. SpaceX, "SpaceX - Starship and Super Heavy," 05 08 2024. [Online]. Available: https://www.spacex.com/vehicles/starship/. [Accessed 20 08 2024].
2. Wilken, J., Callsen, S.: Mission design for point-to-point passenger transport with reusable launch vehicles. CEAS Space J. **16**, 319–332 (2023)
3. Sippel M., Dietlein I., Wilken J., Pastrikakis V., Barannik V and du Toit T.: "System Aspects of European Reusable Staged-Combustion Rocket Engine SLME," in *Space Propulsion 2024*, Glasgow, Schottland U.K., 2024–05–20 (2024)
4. Sippel M., Stappert S., Bussler L. and Forbes-Spyratos S.: "Technical Progress of Multiple-Mission Reusable Launch Vehicle SpaceLiner," in *HiSST 2018–1580839*, 1st HiSST: International Conference on High-Speed Vehicle Science Technology, Moscow, (2018)
5. Sippel M., Stappert S., Bussler L., Singh S. and Krummen S.: "Ultra-Fast Passenger Transport Options Enabled by Reusable Launch Vehicles," in *1st FAR conference*, Monopoli, Italy, (2019)
6. SpaceX, "flickr - Official SpaceX Photos," flickr, 16 04 2023. [Online]. Available: https://www.flickr.com/photos/spacex/. [Accessed 29 01 2025].
7. Sippel M., Stappert S. and Koch A. D.: "Assessment of Multiple Mission Reusable Launch Vehicles," in *69th International Astronautical Congress*, Bremen, Germany (2018)
8. Wilken J., Sippel M. and Berger M.: "Critical Analysis of SpaceX's Next Generation Space Transportation," in *2nd International Conference on High-Speed Vehicle Science Technology (HiSST)*, Bruges, Belgium (2022)
9. Sesnic T.: "Everyday Astronaut: Starbase Tour and Interview with Elon Musk," 11 08 2021. [Online]. Available: https://everydayastronaut.com/starbase-tour-and-interview-with-elon-musk/. [Accessed 01 08 2024].
10. Berger E.:"Elon Musk just gave another Mars speech—this time the vision seems tangible," Ars Technica, 8 4 2024. [Online]. Available: https://arstechnica.com/space/2024/04/elon-musk-just-gave-another-mars-speech-this-time-the-vision-seems-tangible/. [Accessed 14 8 2024].
11. Kayal H.: "Aufbau eines vereinfachten Simulationsmodells für den Bahnaufstieg in der Großkreisebene," 1993. [Online]. Available: https://elib.dlr.de/23152/. [Accessed 27 August 2024].
12. van Foreest A., Sippel M. and Isselhorst A.: "A fast engineering tool for simulation and design of propellant management systems in liquid propelled launcher stages," in EUCASS 2009, Versaille,France (2009)
13. Garbers N.: "Thermal protection system Optimization Program Version 2 (TOP2)," German Aerospace Center, Bremen, (2014)
14. Kopp A. and Bussler L.: "Validierung der Aerodynamik und Aerothermodynamik Analyseprozeduren des Hotsose Codes Version 1.91," DLR-SART, Bremen (2018)
15. Reisch U. and Streit T.: "Surface Inclination and Heat Transfer Methods for Reacting Hypersonic Flow in Thermochemical Equilibrium," *New Results in Numerical and Experimental Fluid Mechanics. Notes on Numerical Fluid Mechanics (NNFM), vol 60.,* p. pp 267–274, 1997.

16. Klevanski J. and Sippel M.: "Beschreibung des Programms zur aerodynamischen Voranalyse CAC Version 2," German Aerospace Center, Bremen, 2003.
17. Ponomarenko A.: "RPA: Design Tool for Liquid Rocket Engine Analysis," January 2009. [Online]. Available: http://rocket-propulsion.info/resources/software/rpa/RPA_LiquidRocketEngineAnalysis.pdf. [Accessed September 2024].
18. Parsley S. D., Peery C. and Joyner R.: "Future Technology Directions and Payoffs for Reusable Cryogenic Propulsion," in *5ème Symposium International, La Propulsion Dans Les Transports Spatiaux*, Paris, 22.-24. Mai 1996.
19. Sesnic T.: "YouTube - Elon Musk Explains SpaceX's Raptor Engine!," 14 7 2022. [Online]. Available: https://web.archive.org/web/20220819095907/https://everydayastronaut.com/spacex-raptor-engine-comparison/. [Accessed 28 5 2024].
20. SpaceX, "Performance Stats of Raptor," 3 08 2024. [Online]. Available: https://x.com/spacex/status/1819795288116330594. [Accessed 5 09 2024].
21. "Wikipedia - SpaceX Raptor," 05 05 2024. [Online]. Available: https://en.wikipedia.org/wiki/SpaceX_Raptor. [Accessed 05 09 2024].
22. SpaceX, "X - Raptor 3 (sea level variant)," 03 08 2024. [Online]. Available: https://x.com/spacex/status/1819772716339339664. [Accessed 12 09 2024].
23. Sippel, M., Wilken, J.: Selection of propulsion characteristics for systematic assessment of future European RLV options. CEAS Space J **17**, 131–154 (2025)
24. Jax, "Feeding The Beast: Super Heavy's Propellant Distribution System," Ringwatchers, 16 12 2023. [Online]. Available: https://ringwatchers.com/article/booster-prop-distribution. [Accessed 1 08 2024].
25. RGV Aerial Photography, RGV Aerial Photography, 2018. [Online]. Available: https://rgvaerial.org/. [Accessed 24 02 2025].
26. Zee, S.M.: Written re-evaluation of the 2022 final programmatic environmental assessment for the SpaceX Starship/Super Heavy launch vehicle program at the Boca Chica launch site in Cameron county, Texas. FAA, USA (2023)
27. Dimian, A.C., Bildea, C.S., Kiss, A.A.: "Generalised computational methods in thermodynamics," in computer aided chemical engineering, pp. 157–200. Elsevier, Netherlands (2022)
28. C. Hime, "X.com - Close Up of the IFT4 Heatshield," Cooper Hime Cinematic Motion Pictures, 08 03 2021. [Online]. Available: https://x.com/Cooper_Hime/status/1369029998934392833. [Accessed 24 02 2025].
29. "Space Exploration Technologies DBA Starship Tile Facility - INSPECTION REPORT FINAL," Florida Department of Environmental Protection, Florida, USA, 2020.
30. Forgsberg, K.: Producing the high temperature reusable surface insulation for the thermal protection system of the Space Shuttle. In: Intern AAAF Aeron Congr on New Develop in Struct and Mater. France, Paris (1979)
31. Rath-Group, "HOCHTEMPERATURWOLLE - Ultraleichtes Isoliermaterial für Wärmedämmung bis 1650°C," 2017. [Online]. Available: https://www.rath-group.com/fileadmin/user_upload/RATH_Hochtemperaturwolle_201710_DE_preview.pdf. [Accessed 23 5 2024].
32. SpaceX, "SpaceX Starship Flight 4 - Reupload by The Launch Pad," The Launch Pad, 06 06 2024. [Online]. Available: https://www.youtube.com/watch?v=eQO9-ILZrH0. [Accessed 2025 01 28].
33. Jax, "Ringwatchers - The Bestagons: Starship's Upgraded Heat Shield," Ringwatchers, 27 12 2024. [Online]. Available: https://ringwatchers.com/article/s33-tps. [Accessed 28 01 2025].
34. SpaceX, "Twitter - IFT2 Stream," 18 11 2023. [Online]. Available: https://x.com/spacex/status/1725852544587727145. [Accessed 24 5 2024].
35. SpaceX, "Twitter - IFT3 Stream," 5 3 2024. [Online]. Available: https://x.com/SpaceX/status/1765037578343121372. [Accessed 24 5 2024].
36. Billington C.: "Starship Telemetry Extractor - Gitlab," 5 2023. [Online]. Available: https://github.com/chrisjbillington/starship_telemetry. [Accessed 7 8 2024].
37. SpaceX, "SpaceX Starship Flight 5 - Reupload by The Launch Pad," The Launch Pad, 13 10 2024. [Online]. Available: https://www.youtube.com/watch?v=eXsT2HT171o. [Accessed 28 01 2025].
38. SpaceX, "SpaceX Starship Flight 7 - Reupload by The Launch Pad," The Launch Pad, 17 01 2025. [Online]. Available: https://www.youtube.com/watch?v=Z_oDjirpBqA. [Accessed 28 01 2025].
39. SpaceX, "SpaceX - Falcon Heavy," 16 November 2012. [Online]. Available: https://web.archive.org/web/20200519020710/https://www.spacex.com/falcon-heavy. [Accessed 5 April 2017].
40. Creech S.: "NASA's Space Launch System: A Capability for Deep Space Exploration," NASA, April 2014. [Online]. Available: https://web.archive.org/web/20160307231643/https://www.nasa.gov/sites/default/files/files/Creech_SLS_Deep_Space.pdf. [Accessed 4 September 2018].
41. NASA, "Saturn V Flight Manuel - SA 507," NASA, Houston, USA, (1969)
42. Sippel, M., Trivailo, O., Bussler, L., Lipp, S., Valluchi, C.: "Evolution of the SpaceLiner towards a Reusable TSTO-Launcher," in International Astronautical Congress 2016. Guadalajara, Mexico (2016)
43. Sippel M., Klevanski J. and Steelant J.: "Comparative Study on Options for High-Speed Intercontinental Passenger Transports: Air-Breathing- vs. Rocket-Propelled," in *IAC-05-D2.4.09*, Fuduoka, Japan, October (2005)
44. Sippel M., Schwanekamp T., Trivailo O., Kopp A., Bauer C. and Garbers N.: "SpaceLiner Technical Progress and Mission Definition," in *AIAA 2015–3582, 20th AIAA International Space Planes and Hypersonic Systems and Technologies Conference*, Glasgow, July (2015)
45. Sippel M., Stappert., Bayrak Y., Bussler L. and Callsen S.: "Systematic Assessment of SpaceLiner Passenger Cabin Emergency Separation Using Multi-Body Simulations," in *2nd HiSST-conference*, Bruges, Belgium, (2022)
46. M. Sippel, J. Wilken, L. Bussler, S. Callsen and Mauriello T.: "Progress in Pre-Definition of the SpaceLiner 8 Advanced Hypersonic Transport," in *HiSST: 3rd International Conference on High-Speed Vehicle Science Technology*, Busan,Korea, (2024)
47. Bussler L. and Sippel M.: "Reference Concept SLB 8 Booster," DLR-SART, Bremen, (2022)
48. Singh S.: "Relative Navigation Implementation for the In-Air Capturing of a Winged Reusable Launch Vehicle," in *HiSST 2024 – 279, 3rd HiSST Conference*, Busan, Korea, (2024)
49. Singh S., Bussler L., Bergmann K. and Sippel M.: "Mission Design and Sensitivity Analysis for In-Air Capturing of a Winged Reusable Launch Vehicle," in *IAC-23-D2.5.5, 74th International Astronautical Congress (IAC)*, Baku, Azerbaijan, October (2023)
50. Wiedemann, J., Acquatella, P., Basken, R., Bozic, O., Bufetti, B., Ettl, J., Glaser, T., Hassenpflug, F., Hecht, M., Hörschgen-Eggers, M., Hrbud, I., Kimpe, A., Klevanski, J.: VLM-1 - Vehicle Design and Analysis (XTRAS-TN-VLM-20150302). DLR, Bremen (2015)
51. Sippel, M., Wilken, J.: "Preliminary component definition of reusable staged-combustion rocket engine," in *Space Propulsion 2018*. Seville, Spain (2018)

52. Sippel, M., Stappert, S., Pastrikakis, V., Barannik, V., Maksiuta, D., Moroz, L.: “Systematic studies on reusable staged-combustion rocket engine slme for european applications,” in *8th Space Propulsion*. Estoril, Portugal (2022)
53. Vila J. and Hassin J.: "Technology acceleration process for the THEMIS low cost and reusable prototype," in *8TH EUROPEAN CONFERENCE FOR AERONAUTICS AND SPACE SCIENCES*, Madrid, (2019)
54. Ishimoto S., Tatiossian P. and Dumont E.: "Overview of the CALLISTO Project," German Aerospace Center, Bremen, (2019)
55. Parsonson A.: "European Spaceflight - ESA Selects Four Companies to Develop Reusable Rocket Technology," 28 10 2024. [Online]. Available: https://europeanspaceflight.com/esa-selects-four-companies-to-develop-reusable-rocket-technology/. [Accessed 21 04 2025].
56. Dietlein, I., Stappert, S., Wilken, J., Bussler, L., Sippel, M.: “Options for future European reusable booster stages: evaluation and comparison of VTHL and VTVL return methods,” *CEAS Space Journal,* vol. CEAS Space Journal **2025**(17), 155–175 (2024)
57. Sippel M., Dietlein I., Herberhold M., Bergmann K. and Bussler L.: "Launcher Options for Europe in a World of Starship," in *IAC-24-D2.4.2, 75th International Astronautical Congress*, Milan, Italy, (2024)

**Publisher's Note** Springer Nature remains neutral with regard to jurisdictional claims in published maps and institutional affiliations.